NUMERICAL STUDY OF IMPROVED METHODS OF IN-FIELD CAPACITY ASSESSMENT OF REINFORCED CONCRETE BRIDGES

BY

MATTHEW B. GRIES

THESIS

Submitted in partial fulfillment of the requirements
for the degree of Master of Science in Civil Engineering
in the Graduate College of the
University of Illinois at Urbana-Champaign, 2010

Urbana, Illinois

Adviser:

Professor Daniel A. Kuchma

ABSTRACT

Bridges, particularly short-span highway bridges, are basic elements of nearly all contemporary transportation networks. For reinforced concrete structures, complete information regarding the number, size, and orientation of steel reinforcement is necessary in order to make a complete strength assessment. Since reinforcement is not visible externally, making an accurate assessment without design drawings is extremely difficult. Improving the accuracy of capacity assessments of reinforced concrete bridges when information regarding the design and construction of the bridge is limited or not available would be useful in a number of situations, including military operations and disaster response. The objective of this project is to develop more reliable means of in-field capacity assessment of reinforced concrete bridges by making improved estimates of the level of longitudinal and shear reinforcement. The proposed assessment procedure is based on comparing measured structural response under controlled loading conditions to predicted structural response from analysis. This report presents results from a preliminary sensitivity study of the analytically predicted response of simply supported reinforced concrete T-beam girders with varying levels of longitudinal and shear reinforcement.

This thesis is dedicated to my mother.

ACKNOWLEDGEMENTS

I thank my adviser, Professor Dan Kuchma for providing the opportunity to perform research at the University of Illinois. I also thank Professor Bill Spencer and Professor Larry Bergman for their collaboration and guidance in this project. I would like to also acknowledge PhD candidate Ryan Giles for his development of the dynamic model used in this project. Additionally, I would like to acknowledge James Wilcoski from the U.S. Army Construction Engineering Research Laboratory and James Ray from the U.S. Army Engineering Research and Development Center for their consultation.

TABLE OF CONTENTS

Chapter 1: Introduction 1
1.1 Background 1
1.2 Problem Statement 2
1.3 Approach 3
Chapter 2: Bridge and Parameter Selection 6
2.1 Bridge Selection 6
2.2 Loadings 7
2.3 Design Requirements 11
2.4 Capacity Evaluation Procedure 14
2.5 Final Bridge Parameters 19
Chapter 3: Static Model 21
3.1 Analytical Tools 21
3.2 Models Used in Assessment 28
3.3 Predicted Responses 31
Chapter 4: Dynamic Model 39
4.1 Models Used in Assessment 39
4.2 Predicted Responses 40
Chapter 5: Approach Evaluation 43
5.1 Sensor Technology Survey 43
5.2 Example Problem 50
Chapter 6: Literature Review of Related Topics 54
6.1 ERDC Multi-Resolution Approach 54
6.2 Flexural Rigidity, EI 55
Chapter 7: Conclusions 58
7.1 Limitations 58
7.2 Future Work 60
7.3 General Conclusions 64
References 65

CHAPTER 1: INTRODUCTION

1.1 Background

Bridges, particularly short-span highway bridges, are basic elements of nearly all contemporary transportation networks. In most developed countries, information regarding the engineered design and as-built construction documents for a majority of the highway bridge inventory is thorough and complete. The advancement of computers and digital documentation has facilitated the ability to preserve this information and make it more readily accessible when needed. Each bridge in a well organized inventory would be assigned a load rating that corresponds to largest vehicle allowed to pass the structure under normal traffic conditions. For everyday vehicles, this load rating may be governed by fatigue concerns in the structure. Less frequent and more demanding vehicles, called permit loads, are granted special permission by the governing body to pass over a given bridge or highway route. Generally these permit loads are allowed based on an assessment of the strength of the structure. Usually permits loads are familiar and obtaining permission is more of an administrative formality; however, there do exist certain permit loads which require special attention and a structural assessment based on the as-built construction documents.

For reinforced concrete bridges, having accurate information regarding the as-built details of the structure is especially important. In steel structures, the structural elements are generally visible externally; thus visual inspection and measurement of structural members provide much of the critical information needed to make an accurate structural assessment when accurate as-built drawings are not available. However, in reinforced concrete structures, complete information regarding the number, size, and orientation of steel reinforcement is necessary in order to make a complete strength assessment. Since reinforcement is not visible externally, making an accurate assessment without as-built construction drawings is extremely difficult. Currently, when the United States (U.S.) military performs capacity assessments of reinforced concrete bridges with little or no information about the design and construction of the bridge, their assessment is based on conservative assumptions, which generally underestimate load carrying capacity (U.S. Army, 2002; Ray & Butler, 2004).

Improving the accuracy of capacity assessments of reinforced concrete bridges when information regarding the design and construction of the bridge is limited or not available would be useful in a number of situations. One beneficiary from an improved means of reinforced concrete bridge assessment would be the U.S. military. In wartime operations, the U.S. military encounters bridges and must determine if their large tanks and heavy equipment transporter systems are safe for passage. To complicate matters, highways systems in many countries often have been developed over the last century by various foreign interests to different design standards. Thus, assumptions regarding the types of loads and requirements

used in design may not be valid. In addition to wartime operations, the military and other organizations involved in disaster response could benefit as well. In response to natural disasters such as an earthquake or tornado, communication is often hindered and transportation systems limited. In these situations, it is critical that relief supplies be transported safely and effectively. Having more accurate means of making in-field bridge assessments when communication is limited and design documents are unavailable helps ensure that supplies is transported safely without being unnecessarily hindered by overly conservative assumptions. Finally, improved methods of capacity assessment could improve the robustness of bridge inventories when information is missing due to lack of documentation.

1.2 Problem Statement

The objective of this project is to develop more reliable means of in-field capacity assessment of reinforced concrete bridges by making improved estimates of the level of longitudinal and shear reinforcement. The assessment procedure, outlined in Section 1.3, is based on comparing measured structural response under controlled loading conditions to predicted structural response from analysis. This report presents results from a sensitivity study of the analytically predicted response of simply supported reinforced concrete T-beam girders to varying levels of longitudinal and shear reinforcement. The outline for this report is presented below.

Chapter 1 discusses the motivation for developing an improved method of in-field capacity assessment of reinforced concrete bridges. In this chapter, the proposed approach is outlined.

Chapter 2 introduces the selected structure which served as the basis for analysis as well as the loads used throughout this study. Discussion regarding the challenges behind identifying the standard code of practice by which a given bridge was designed is presented. Additionally, a capacity evaluation approach is presented along with the final parameters used in this sensitivity study.

Chapters 3 and 4 introduce the models used in the static and dynamic analysis, respectively. The static models and analysis are discussed in detail and reflect the research performed by the author of this paper. The dynamic models and analysis, which was developed by a colleague (Gries, Giles, Kuchma, Spencer, & Bergman, 2010), is presented at a high level and is meant to supplement the detailed static analysis to present a more complete understanding of the goals of the ongoing research.

Chapter 5 provides a high-level introductory survey of various sensor technologies with potential application to this project. A hypothetical example of the proposed method of capacity assessment is discussed to provide context to the results of Chapter 3.

Chapter 6 summarizes the results from a literature review of previous research of topics related to the work presented in this report. Summary of a multi-resolution assessment methodology developed by the U.S. Army Engineering Research and Development Center (ERDC) is presented. Additionally,

discussion regarding methods of determining the flexural stiffness, EI, of a reinforced concrete beam is presented.

Chapter 7 discusses the limitations and assumptions of this report. Conclusions are drawn on the work completed to date and potential future research necessary to further develop this method for practical field application is discussed.

1.3 Approach

In order to place appropriate bounds on this preliminary numerical study to isolate key variables and identify areas of high potential for future research and development, this study necessarily limits itself with a number of assumptions. As further discussed in Section 2.1, the class of structures analyzed in this project is limited to simply supported reinforced concrete T-beam girders. This class of structures was selected due to its applicability to a broad spectrum of geographic locations. Additionally, simply supported T-beam girders allow for more direct insight into the behavioral response of the structure due to its boundary conditions. It is possible that the concepts and analyses explored in this report could be expanded to applications for other types of structures such as reinforced concrete girders which act continuously between spans.

In addition to the class of structure, it is assumed in this study that there exists complete information regarding the geometry of the structure. Specifically, it is assumed that the span length and cross section dimensions are all known. Programmatically, in terms of field application, there would have to be sufficient access to the structure to obtain this information. It is also assumed that moment and shear demands on the member are known. This requires sufficient understanding of both the dead and live load demands. For dead load, this means that the self weight is calculated from the known cross section geometry and the superimposed dead load is understood based on asphalt overlays, railings, sidewalks, etc. For live load, the vehicle axle loads and axle spacings are known. Based on distribution factors and influence lines, the demands that these vehicles impose on individual members are known. More detailed discussion regarding the limitations and assumptions associated with this project is located in Section 7.1 of this report.

In order to make improved estimates of the levels of longitudinal and shear reinforcement in the structure, it is critical to understand what quantities are known and unknown. The noted assumptions underlying the project identify that the known quantities consist of the member geometry and demands imposed on the analyzed girder. The isolated unknown quantities become the levels of shear and longitudinal reinforcement. To accurately assess the levels of reinforcement, this project compares predicted member response to member response measured in the field. Member response includes behavior such as deflections, curvature, strains, and accelerations due to vibration. The predicted

member response for assumed levels of reinforcement is determined through the use of nonlinear analysis programs, which are described in further detail in Chapters 3 and 4. The nonlinear analysis tools are capable of analyzing both static and dynamic member response. The measured member response is possible through the use of various sensor technologies such as extensometers, laser measurement systems, and photogrammetry. A survey of current sensor technologies is provided in Section 5.1.

In order to more clearly understand the aim of this project and how it could potentially be implemented in the field, the following briefly outlines the procedure steps:

1. *Determine critical demand* – This step requires identifying the most demanding vehicle that is desired to be passed across the bridge. It is necessary to identify what load rating will be required for the structure based on the largest demand that will be imposed on the structure. Assessing the demand on the structure includes identifying the maximum bending moment and shear demand as a combination of dead and live load. Finding these demands may incorporate the use of impact factors to account for dynamic amplification and factors of safety for dead and live loads.

2. *Assess critical level of longitudinal and shear reinforcement* – This step identifies the minimal allowable level of reinforcement that would allow passage of the critical demand. In this report, identification of the critical level of reinforcement is determined through the procedure outlined in Section 2.4, which is based on common American Association of State Highway and Transportation Officials (AASHTO) design principles and a standardized classification system for assigning load rates.

3. *Predict member response* – Through the use of non-linear static and dynamic analysis, this step predicts the response of the girder loaded with a less demanding vehicle than the vehicle identified in Step 1. In addition to analyzing the member for the critical level of reinforcement, analysis is performed for levels of reinforcement greater than and less than the critical level to create a gradient of responses.

4. *Measure member response* – In the field, the vehicle used in the predictive analysis is driven over the structure and the actual member response is measured through the use of sensor technologies. Key aspects of the response include deflections, strains, accelerations, etc.

5. *Compare measured and predicted responses* – By comparing the measured responses to the predicted responses, insight is gained into whether the level of reinforcement in the structure is above or below the critical level of reinforcement described in Step 2.

Once adequate information regarding the level of reinforcement in the structure is determined, current methods of assessing the bridge's adequacy for vehicle passage can be used; thus further development of Steps 1 and 2 are outside the scope of this project. This project describes a hypothetical, but reasonably applicable, situation for Steps 1 and 2 and then performs the detailed analysis associated with Step 3. The project proceeds to make inferences regarding the feasibility of Steps 4 and 5.

CHAPTER 2: BRIDGE AND PARAMETER SELECTION

2.1 Bridge Selection

In order to effectively study differences in bridge behavior due to the level of reinforcement, a bridge needed to be selected to serve as the basis for analysis. Based on the potential beneficiaries from the development of a more accurate bridge assessment procedure, it was determined that the analyzed bridge should represent structures commonly experienced in military operations, but should not be exclusive to a specific geographic location. That is, the selected structure should provide insight into bridge evaluation that can be applied to a general class of bridges. To this end, it was determined that analysis of simply supported T-beam girders would be most appropriate. Bridges with simply supported T-beam girders are common along developed highway routes throughout the world.

The bridge selected for analysis in this report, shown in Figure 2.1, contains seven parallel girders spaced at 120 cm center to center. Each girder is 90 cm in depth, with the 20 cm thick flange consisting of a 10 cm thick cast in place concrete slab on top of a 10 cm thick precast flange. The 70 cm deep web has a width of 20 cm. The span is 13.9 meters in length, simply supported on 55 cm wide steel bearing plates (12.8 m clear span).

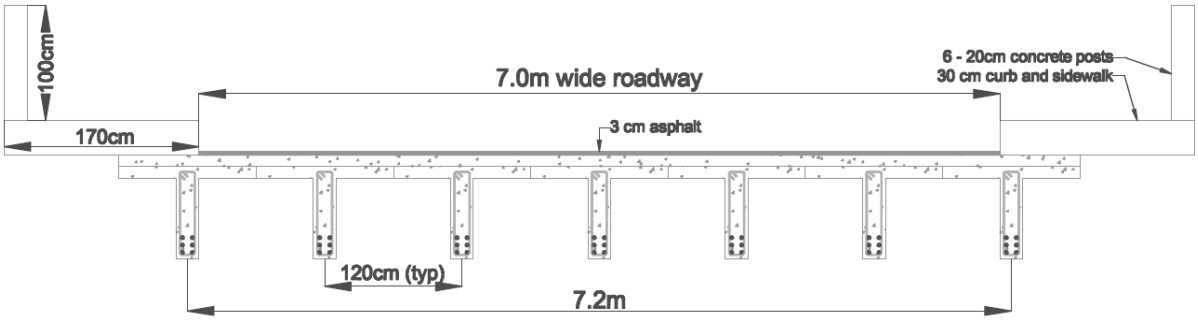

Figure 2.1: Cross section diagram of analyzed bridge

This study analyses the behavior of a single girder from this bridge. The girder reinforcement details in Figure 2.2 represent a common level and orientation of reinforcement for a modern highway bridge of this span length. Flexural reinforcement consists of six 32 mm diameter deformed bars. Shear reinforcement was determined to consist of two legs of 12 mm diameter stirrups spaced at 15 cm o.c..

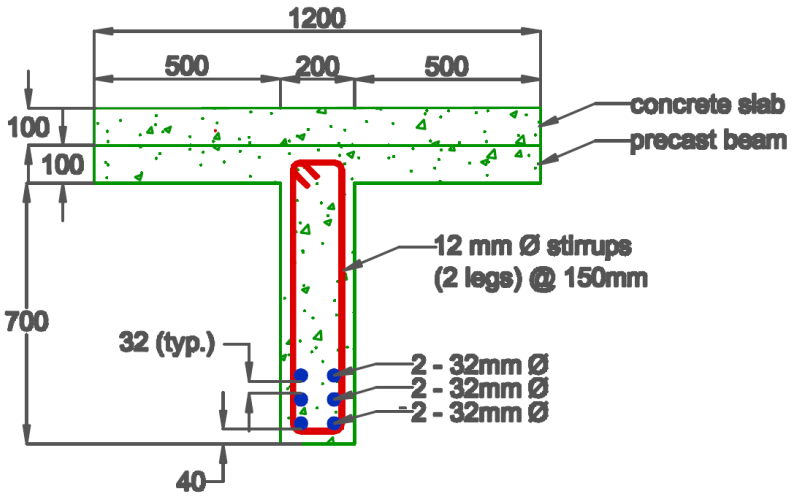

Figure 2.2: Cross section of analyzed girder (all units mm)

Material properties used in analysis are also based on experience with this size and class of bridge. The concrete compressive strength of the precast beam is 30 MPa (4350 psi), while the compressive strength of the concrete slab is 21 MPa (3000 psi). The yield strength of the steel reinforcement is 350 MPa (50 ksi).

2.2 Loadings

When analyzing the structure, a number of different load conditions are considered. As previously discussed, the proposed assessment methodology is expected to potentially benefit the military. To relate the study to military operations, three primary vehicles were considered and referenced throughout the analysis. These vehicles were selected to be representative of the types of vehicles that would be commonly found in military convoy operations. The lightest military vehicle considered was the High Mobility Multipurpose Wheeled Vehicle (HMMWV), with an assumed weight of 3 tons. In this project, the HMMWV serves to induce vibration in the dynamic modeling and analysis. The second military vehicle referenced in this project is the M1-ABRAMS tank. The weight of the M1-ABRAMS tank can vary depending on the level of armor and the type of carried equipment, however, the tank referenced in this project evenly distributes 80.5 tons over 7 axles (Figure 2.3). The M1-ABRAMS serves as the intermediate load used in static analysis of the structure. The third military vehicle considered is the Heavy Equipment Transporter System (HETS), commonly referred to as a tank carrier. This heavy, wheeled vehicle is identified as the most demanding vehicle that is desired to be passed across the bridge, i.e. the criteria for which the critical level of longitudinal and shear reinforcement is determined. The HETS tank carrier weighs 137.8 tons, distributed over 9 axles (Figure 2.4).

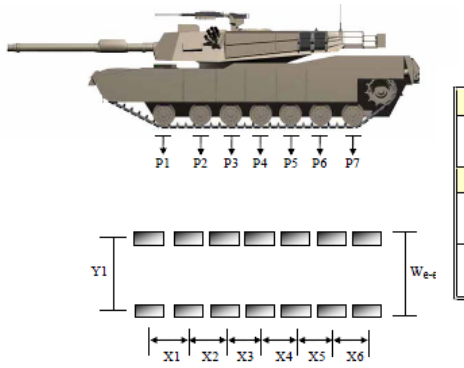

Loading Data							
Axle Weights (k)	P1	P2	P3	P4	P5	P6	P7
	23.0	23.0	23.0	23.0	23.0	23.0	23.0
Dimensions							
Transverse Spacing (ft)	W_{e-e}	Y1					
	11.42	9.34					
Longitudinal Spacing (ft)	X1	X2	X3	X4	X5	X6	
	3.0	2.4	2.4	2.4	2.4	2.44	

Figure 2.3: M1-ABRAMS Tank Load Distribution

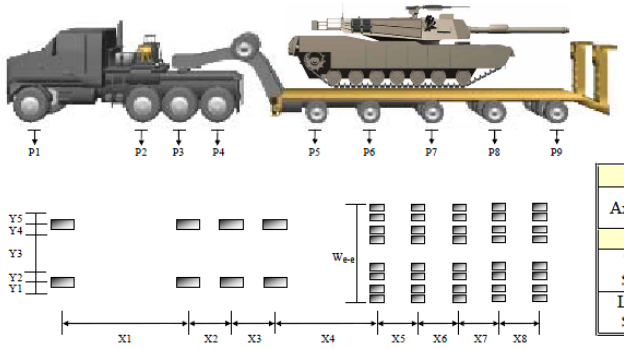

Loading Data									
Axle Loads (k)	P1	P2	P3	P4	P5	P6	P7	P8	P9
	6.25	6.25	6.0	5.6	8.2	8.2	8.2	10.1	10.1
Dimensions									
Transverse Spacing (ft)	W_{e-e}	Y1	Y2	Y3	Y4	Y5			
	12.0	1.67	1.12	4.85	1.12	1.67			
Longitudinal Spacing (ft)	X1	X2	X3	X4	X5	X6	X7	X8	
	12.92	5.00	5.00	15.08	5.94	5.94	5.94	5.94	

Figure 2.4: HETS Load Distribution

In order to evaluate the cracked state of the girder, highway design loads were considered as the load history of the structure. In the analysis, consideration was given to service loads as well as permit loads. The service load that governed in analysis was the AASHTO HS20-44 truck, which weighs 36 tons, distributed between 3 axles (Figure 2.5). To capture the effect of larger permit loads, the California Permit Truck, shown in Figure 2.6, was considered. While this permit truck contains 8 heavily loaded axles, the simply supported span of the analyzed structure would allow at most 3 axles imposing demand on the girder.

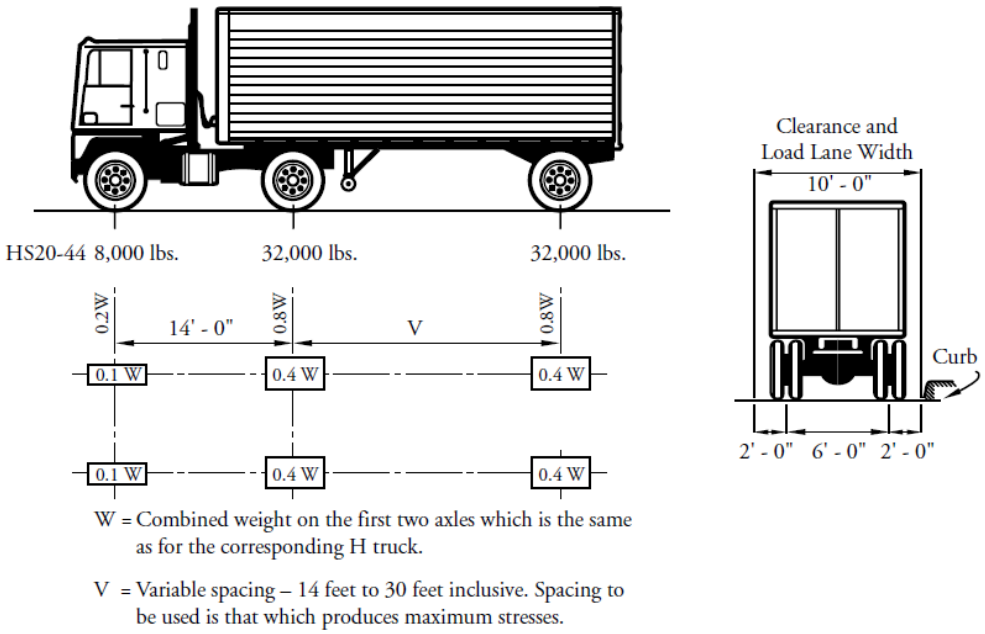

Figure 2.5: AASHTO HS20-44 Truck (Precast/Prestressed Concrete Institute, 2003)

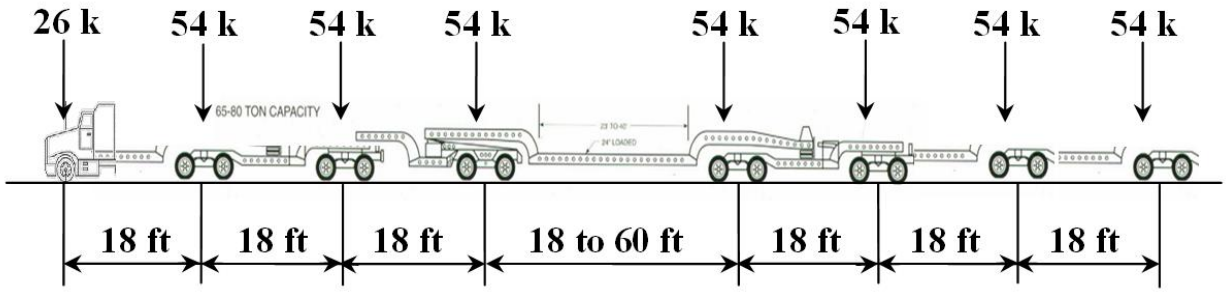

Figure 2.6: California Permit Truck (Caltrans, 2008)

In order to standardize the process of rating a bridge based on load carrying capacity, the military adheres to a classification system established by the North Atlantic Treaty Organization (NATO). This classification system was designed for military vehicles and represents the vehicle's load effect on a bridge. A given vehicle is assigned a military load classification (MLC), which represents a combination of factors including gross weight, axle spacing, axle width, and weight distribution to the axles. The number in the MLC loosely correlates to the weight of the vehicle, but it is important to understand that the MLC represents other factors as well. This classification system also distinguishes between tracked and wheeled vehicles, for example, a 40 ton tank might be classified as a T40, while a W40 corresponds to a wheeled vehicle with a gross weight of 47 tons (NATO, 1990; Van Groningen & Paddock, 1997).

Through the load rate analysis described in Section 2.4, a bridge is assigned one or more MLC corresponding to the largest tracked or wheeled vehicle allowed to pass under one-way or two-way

crossing procedures. Generally, the bridge MLC assumes that the vehicles on the bridge are spaced at a minimum of 100 feet and traveling at a maximum speed of 25 miles per hour. When convoys are unrestricted and allowed to use the normal traffic lanes, this crossing procedure is referred to as normal crossing. A caution crossing procedure is used in special cases where a bridge is not rated high enough at the normal crossing level for the desired vehicle MLC. Caution crossing requires one-way crossing along the centerline of the bridge, with vehicles spaced at 150 feet. Vehicles are limited to a maximum speed of 8 mph, with no braking or shifting during passage. A summary of the special crossing considerations are outlined in Table 2.1, including risk crossing which is not considered in this report. (U.S. Army, 2002)

Table 2.1: FM3-34.343 Table 5-1; Special-Crossing Considerations (U.S. Army, 2002)

Considerations	Type of Crossing		
	Normal	Caution	Risk
Classification	As posted	Standard bridges: as published	Standard bridges: as published
		Nonstandard bridges: 125 percent of normal one-way classification	Nonstandard bridges: no crossing
Spacing	100 feet	150 feet	One vehicle on bridge at a time
Speed	25 mph	8 mph	3 mph
Location	In lane	Bridge centerline	Bridge centerline
Other	None	No stopping, braking, or accelerating	No stopping, braking, or accelerating; inspect the bridge after each crossing

For the selected bridge, a load rate analysis determined the following load ratings for normal crossing levels:

2-way traffic:

- Wheeled MLC = W60
- Tracked MLC = T60

1-way traffic:

- Wheeled MLC = W80
- Tracked MLC = T70

Similarly, a load rate analysis determined the following load ratings for caution crossing levels:

1-way traffic:

- Wheeled MLC =W90
- Tracked MLC = T80

Based on the standard classification methodology for assigning a vehicle MLC, the HETS rates as a class W96 up to W101. However, it is recognized that the methodology may be overly conservative for this specific vehicle due to its multi-axle and multi-wheeled configuration. To determine a more accurate rating for the HETS, an extensive 3-year study was performed by the U.S. Military Traffic Management Command Transportation Engineering Agency (MTMCTEA), in partnership with the Federal Highway Administration (FHWA) and contracted with New Mexico State University (NMSU). This study performed over 400 computer simulated analyses to determine the critical bending moments on bridges ranging in span from 20 to 140 feet. Bridge dimensions for the computer analysis were determined through the evaluation of a large database of existing bridges. Results from analysis were verified through field tests conducted by NMSU and the Texas and Colorado Departments of Transportation. Based on this study, for a bridge of the same span as the selected structure, the equivalent MLC for the HETS is W49. (Minor & Woodward, 1999)

2.3 Design Requirements

It is important to understand that the standards and codes by which bridges and other reinforced concrete structures were designed and constructed have evolved as understanding of reinforced concrete structures has developed through research and design experience. The two principal codes which are currently utilized in the United States for design of reinforced concrete structures are the American Concrete Institute (ACI) Building Code and the American Association of State Highway and Transportation Officials (AASHTO), formerly the American Association of State Highway Officials (AASHO), LRFD Highway Bridge Specifications. Current highway bridge design in the United States is based on AASHTO design standards, which makes reference to a number of the provisions in the ACI Building Code.

When looking at the changes in ACI design since its first publication in 1910, there exist both changes in an overall design philosophy as well as specific changes in addressing reinforcement requirements, especially for shear resistance. Prior to 1963, the ACI code exclusively used working stress design as its design philosophy. The working stress design limits the maximum elastically computed stresses at service loads to be less than the material strengths by a factor of safety. This approach assumes that ultimate limits states, such as rupture, formation of plastic mechanism, instability, or fatigue, are automatically satisfied. However, MacGregor and Wight point out that this is not necessarily the case, and points to the following major drawbacks to working stress design (2005):

- Inability to account for variability of loads and resistance
- Lack of knowledge of the level of safety (with respect to ultimate limit states)
- Inability to deal with load combinations where load rates are not the same

In 1963, the ACI code introduced the ultimate strength design approach in addition to the working stress design approach. In ultimate strength design, factored load combinations and capacity reduction factors are applied to proportion members based on calculations of ultimate strength. In addition to developing a stronger sense of the overall safety of members, serviceability is accounted for through provisions for control of deflections and cracking under service loads. After its introduction in 1963, ultimate strength design quickly became the preferred method of design and working stress design was eventually moved into an appendix and finally removed from the ACI code entirely in 2002.

Prior to the 1951 ACI provisions, ACI shear provisions recognized that shear resistance in beams and girders consisted of both a reinforcement and concrete component. The concrete component of shear resistance was based on experimental tests of members with little to no web reinforcement, and its allowable stress for longitudinal reinforcement with no special anchorage conditions was limited to $0.02f'_c$. Thus, the shear force resisted by the concrete was equal to $0.02f'_c b(jd)$ where b is the width of the web and jd is the flexural lever arm. If stirrups are used to resist shear, the required vertical shear reinforcement area is determined by

$$A_v = \frac{V's}{f_v jd}$$

where

A_v = total area of web reinforcement within a distance s (i.e. combined area of legs of stirrup)

V' = total shear minus the contribution from concrete

s = spacing of stirrups ($\leq$ d/2)

f_v = tensile unit stress of steel

Additionally, a limit on the allowable shear stress at service loads was imposed to prevent a diagonal crushing failure before the yielding of the stirrups. However, it is important to note that through 1951, no shear reinforcement was required if the shear stress at a section was less than the resistance contribution from concrete. That is, no provisions existed for a required minimum level of shear reinforcement. A required minimum level of shear reinforcement of 0.15% was introduced in the 1956 code as a direct response to a 1955 shear failure of beams in the warehouse at the Wilkins Air Force Depot in Shelby, OH (Ramirez, 2009). The requirement for a minimum level of shear reinforcement has been modified over the years as research in response to the 1955 shear failure has refined the level of understanding of shear behavior in beams. Currently, the minimum required level of shear reinforcement is expressed as $0.75\sqrt{f'_c}/f_y$ (ACI Committee 318, 2008). The current minimum requirement is significantly less than that on 1956, as shown in Table 2.2, reflecting that the 1956 provision was a

conservative response to the 1955 failure and that refinement of the code has resulted in a less stringent requirement today.

In addition to changes in the minimum level of shear reinforcement, the allowable design value for the concrete contribution to shear resistance has also evolved. Today, the concrete unit stress, $v_c = 2\sqrt{f'_c}$ (ACI Committee 318, 2008) is considerably larger than the value in 1956, as seen in Table 2.2.

Table 2.2: Comparison of ACI Shear Provisions 1956 & 2008

ACI Comparison 1956 - 2008				
f'c (psi)	Concrete Contribution to Shear Resistance, v_c (psi)		Minimum Level of Shear Reinforcement (%)	
	1956 $0.02f'_c$	2008 $2v(f'_c)$	1956 0.15%	2008 $0.75\sqrt{(f'_c)}/f_y$*
3000	60.0	109.5	0.15%	0.07%
3500	70.0	118.3	0.15%	0.07%
4000	80.0	126.5	0.15%	0.08%
4500	90.0	134.2	0.15%	0.08%
5000	100.0	141.4	0.15%	0.09%
5500	110.0	148.3	0.15%	0.09%
6000	120.0	154.9	0.15%	0.10%

*f_y = 60000 psi

The AASHTO Highway Bridge Specifications have slowly adopted the principal ACI provisions. Two important milestones in the history of the AASHTO provisions as they relate to current practice include the introduction of the HS20-44 design vehicle in 1944 and the full adoption of the ACI shear provisions in 1973. Prior to 1973, bridges designed by AASHTO specifications were not necessarily consistent in their design approaches.

Table 2.3: Timeline of Major ACI and AASHTO Developments

	ACI Building Code	Year	AASHO/AASHTO Highway Bridge Specifications
Working-stress design	First published code	1910	
		1914	AASHO founded
		1944	HS 20-44 loading introduced
	Minimum shear reinforcement introduced	1956	
Ultimate strength design	Introduction of limit state design Revisions to min. shear	1963	
		1974	Fully adopted ACI shear provisions

In trying to understand the design requirements to which a bridge was designed and constructed one would need to have an understanding of the age of the structure as well as to what standard the bridge was designed. Different countries and governments have adopted various codes; some countries have developed their own design standards, some have adopted the U.S. standards, while other less developed regions have no formalized design standards or practices. It is also important to note that many countries' infrastructure have been developed by foreign interests, thus a structure located in one country may have been designed to a standard or code adopted by a foreign country. Even within a particular region, different sections of highways may have been funded by different sources and thus designed by different codes of practice. Additionally, as discussed in the context of ACI and AASHTO code history, the standards to which a structure is developed is very time sensitive. Shear requirements for beams and girders designed to ACI standards vary significantly before and after 1956. Due to difficulty in determining a structure's age from visual inspection, knowing which version of a given code was used in design is further complicated. In short, determining the code of practice used in the design of a bridge is difficult without having detailed information regarding when and by whom the structure was designed and constructed.

2.4 Capacity Evaluation Procedure

For the selected structure, a load rate analysis has been performed in accordance with standard AASHTO and American Concrete Institute (ACI) provisions. In this document, nominal load carrying capacity for shear and bending moment are computed. Once the nominal capacity of the structure is determined, the capacity available to resist live load can be evaluated in terms of military load classification. This load rate analysis procedure finds the capacity of the structure available to carry live load through the following equation (AASHTO, 1994)

$$L = \frac{C - A_1 * D}{A_2 * (1 + I) * DF}$$

where

L = live load effect (the available capacity to resist live load, M_{LL} or V_{LL})

C = member ultimate capacity (M_u or V_u)

D = dead load demand (M_{DL} or V_{DL})

A_1 = dead load factor of safety

A_2 = live load factor of safety

$1 + I$ = impact factor

DF = distribution factor

An example calculation for the level of reinforcement described in Section 2.1 is presented. U.S. customary units are utilized throughout this example in order to present empirical ACI equations in their more recognizable form.

Member ultimate capacity (M_u or V_u)

To determine the bending moment carrying capacity of a girder in the bridge, it is first assumed that the neutral axis depth (c) would be less than 4 inches, thus occurring in the concrete slab which was assumed to have a compressive strength (f'_c) of 3 ksi. By looking at the equilibrium of the section at the point of yield in the longitudinal reinforcement, it is seen:

$$T = C$$

$$A_s * f_y = 0.85 * f_c' * b * a$$

$$a = \frac{A_s * f_y}{0.85 * f_c' * b} = \frac{7.72in^2 * 50ksi}{0.85 * 3.0ksi * 47in} = 3.179in$$

$$c = \frac{a}{\beta_1} = \frac{3.179}{0.85} = 3.74in < 4in$$

Thus, the neutral axis depth assumption is verified. By summing moments about the depth of the compressive stress resultant, the nominal moment carrying capacity is determined by

$$M_n = A_s * f_y * \left(d - \frac{a}{2}\right) = 7.62in^2 * 50ksi * \left(30.77in - \frac{3.18in}{2}\right) * \frac{1ft}{12in} = 926.47ft - k$$

and the ultimate bending strength (M_u) is determined by multiplying the nominal moment capacity by $\varphi_b = 0.90$ to obtain

$$M_u = 0.90 * 926.47 = 833.82ft - k$$

The nominal shear capacity of the girder is the sum of the contributions of the concrete and vertical stirrups to shear resistance. Thus

$$V_n = V_c + V_s$$

where

$$V_c = 2 * \sqrt{f_c'} * b_w * d$$

$$V_c = \left(2 * \sqrt{4350\ psi} * 8\ in * 26.77\ in\right) + \left(2 * \sqrt{3000\ psi} * 8\ in * 4\ in\right) = 31{,}755lb = 31.76k$$

and

$$V_s = \frac{A_s * f_y * d}{s} = \frac{2 * 0.2in^2 * 50ksi * 30.77in}{6in} = 102.56k$$

thus

$$V_n = 31.76k + 102.56k = 134.32k$$

and the design shear capacity (V_u) is determined by multiplying by $\varphi_s = 0.85$ to obtain:

$$V_u = 0.85 * 134.32k = 114.17k$$

Dead load demand (M_{DL} / V_{DL})

Figure 2.1 shows the elements of the bridge that contribute to the dead load calculations. Dead load calculations account for both self weight of the structural members as well as the weight of the superimposed dead loads. The self weight contribution to the dead load includes the weight of the precast concrete girders and cast-in-place concrete slab. Superimposed dead loads account for the weight of the 1.2" thick asphalt overlay, 6" concrete sidewalk, and assumed weight of the railing. The final dead load on an individual girder is calculated to be 0.831 kips/ft. Due to the simply supported boundary conditions, the maximum moment (at midspan) and maximum shear (at support) is calculated as:

$$M_{DL} = \frac{wl^2}{8} = \frac{\left(0.831\frac{k}{ft}\right) * (43.8\ ft)^2}{8} = 194.24ft - k$$

$$V_{DL} = \frac{wl}{2} = \frac{\left(0.831\frac{k}{ft}\right) * (43.8ft)}{2} = 18.54\ k$$

Dead/live load factors of safety (A_1/A_2)

Based on AASHTO guideline, this report utilizes a factor of safety of 1.3 for both dead and live loads (Taly, 1998).

Impact factor (1+I)

Based on the U.S. Army guidelines, this report utilizes an impact factor of 1.15 for normal crossing procedures; 1.0 for caution crossing procedures (U.S. Army, 2002).

Distribution Factor (DF)

The distribution factors used in this report are based on the recommendations of the Army and AASHTO and are calculated based on the spacing of the girders and the type of structural system (AASHTO, 1994; U.S. Army, 2002). For the selected bridge, the concrete deck on concrete T-beams, with a girder spacing of 3.92 ft, the distribution factors were determined to be

- $DF = S/6 = 3.92/6 = 0.603$; moment, 1-way traffic
- $DF = S/6.5 = 3.92/6.5 = 0.653$; moment, 2-way traffic
- $DF = 1.00$; shear

Thus, for moment carrying capacity under normal one-way crossing, M_{LL} was determined by

$$L = \frac{C - A_1 * D}{A_2 * (1 + I) * DF} = \frac{(833.82ft - k) - 1.3 * (194.24ft - k)}{1.3 * (1.15) * 0.603} = 644.83ft - k$$

Once the capacity available to resist live load has been determined, this allowable live load demand is translated into an equivalent MLC based on the span length of the girder. To find the equivalent MLC based on moment, Table 2.4 is double interpolated by entering the table with the span length and two times the live load effect, M_{LL} (to account for both wheel lines).

Table 2.4: FM3-34.343 Table B-2; shear live load effect based on span and MLC (U.S. Army, 2002)

Class	Wheeled/ Tracked	Span Length (feet)									
		35	40	45	50	55	60	70	80	90	100
40	W	442.00	553.00	671.00	788.00	905.00	1,022.00	1,257.00	1,493.00	1,728.00	1,962.00
	T	580.00	680.00	780.00	880.00	980.00	1,080.00	1,280.00	1,480.00	1,679.00	1,880.00
50	W	511.00	656.00	800.00	945.00	1,090.00	1,235.00	1,525.00	1,814.00	2,100.00	2,390.00
	T	713.00	838.00	962.00	1,087.00	1,212.00	1,338.00	1,588.00	1,837.00	2,090.00	2,340.00
60	W	584.00	740.00	914.00	1,089.00	1,263.00	1,438.00	1,786.00	2,140.00	2,490.00	2,840.00
	T	840.00	990.00	1,140.00	1,290.00	1,440.00	1,590.00	1,890.00	2,190.00	2,490.00	2,790.00
70	W	688.00	856.00	1,057.00	1,257.00	1,458.00	1,658.00	2,060.00	2,460.00	2,870.00	3,270.00
	T	963.00	1,138.00	1,312.00	1,478.00	1,662.00	1,837.00	2,190.00	2,540.00	2,890.00	3,240.00
80	W	786.00	936.00	1,103.00	1,332.00	1,561.00	1,790.00	2,250.00	2,710.00	3,170.00	3,630.00
	T	1,080.00	1,280.00	1,480.00	1,680.00	1,880.00	2,080.00	2,480.00	2,880.00	3,280.00	3,680.00
90	W	884.00	1,053.00	1,242.00	1,499.00	1,757.00	2,010.00	2,530.00	3,050.00	3,560.00	4,080.00
	T	1,193.00	1,418.00	1,643.00	1,867.00	2,090.00	2,320.00	2,770.00	3,220.00	3,670.00	4,120.00
100	W	953.00	1,140.00	1,328.00	1,543.00	1,828.00	2,110.00	2,690.00	3,260.00	3,830.00	4,410.00
	T	1,300.00	1,550.00	1,800.00	2,050.00	2,300.00	2,550.00	3,050.00	3,550.00	4,050.00	4,550.00
120	W	1,143.00	1,368.00	1,593.00	1,851.00	2,195.00	2,540.00	3,230.00	3,910.00	4,600.00	5,290.00
	T	1,500.00	1,800.00	2,100.00	2,400.00	2,700.00	3,000.00	3,600.00	4,200.00	4,800.00	5,400.00
150	W	1,297.00	1,562.00	1,827.00	2,092.00	2,405.00	2,830.00	3,670.00	4,520.00	5,560.00	6,210.00
	T	1,725.00	2,100.00	2,478.00	2,850.00	3,230.00	3,600.00	4,350.00	5,100.00	5,850.00	6,600.00

For example, for normal 1-way crossing, M_{LL} was determined to be 644.83 ft-k for a single wheel line. Thus, for the total vehicle, M_{LL} = 1289.66 ft-k and L = 43.8 feet, the calculation of MLC, the following information is read from the chart:

- for L = 40ft, MLC W100 is 1140 ft-k
- for L = 45ft, MLC W100 is 1328 ft-k
- for L = 40ft, MLC W120 is 1368 ft-k
- for L = 45ft, MLC W120 is 1593 ft-k

For MLC = W100, M_{LL} for L = 43.8 ft is found as

$$\frac{1328 - 1140\ ft - k}{45 - 40\ ft} * (43.8 - 40\ ft) + 1140 ft - k = 1282.88\ ft - k$$

For MLC = W120, M_{LL} for L = 43.8 ft is found as

$$\frac{1593 - 1368\ ft - k}{45 - 40\ ft} * (43.8 - 40\ ft) + 1368 ft - k = 1539.00\ ft - k$$

Thus, for L = 43.8 ft and M_{LL} = 1289.66 ft-k, the MLC is found by

$$\frac{120 - 100}{1539 - 1282.8\ ft - k} * (1289.66 - 1282.8\ ft - k) + 100 = 100.54$$

Which is rounded down to 100, thus the MLC based on moment for normal 1-way crossing is W100. Note that this is not the governing rating expressed in Section 2.2. A similar procedure is used for determining the MLC based on shear, which utilizes Table 2.5.

Table 2.5: FM3-34.343 Table B-3; shear live load effect based on span and MLC (U.S. Army, 2002)

Class	Wheeled/ Tracked	Span Length (feet)										
		30	35	40	45	50	55	60	70	80	90	100
40	W	28.93	30.51	31.70	32.62	33.36	34.42	35.47	37.11	38.35	39.31	40.08
	T	32.00	33.14	34.00	34.67	35.20	35.64	36.00	36.57	37.00	37.33	37.60
50	W	34.67	36.86	38.50	40.31	42.08	43.53	44.73	46.63	48.05	49.16	50.04
	T	39.17	40.72	41.88	42.78	43.50	44.09	44.58	45.36	45.94	46.39	46.75
60	W	39.93	42.09	45.45	47.29	48.76	49.96	51.43	54.09	56.08	57.62	58.86
	T	46.00	48.00	49.50	50.67	51.60	52.36	53.00	54.00	54.75	55.33	55.60
70	W	45.97	49.40	51.98	53.98	55.58	56.89	58.22	61.40	63.79	65.64	67.13
	T	52.50	55.00	56.88	58.33	59.50	60.46	61.25	62.50	63.44	64.17	64.75
80	W	49.20	53.26	56.60	59.20	61.28	62.98	64.40	66.63	69.70	72.18	74.16
	T	58.67	61.72	64.00	65.78	67.20	68.36	69.33	70.86	72.00	72.89	73.60
90	W	55.35	59.91	63.68	66.60	68.94	70.85	72.45	74.96	78.41	81.20	83.43
	T	64.50	68.14	70.88	73.00	74.70	76.09	77.25	79.07	80.44	81.50	82.35
100	W	60.02	64.57	69.00	72.44	75.20	77.45	79.33	82.29	84.69	88.06	90.75
	T	70.00	74.28	77.50	80.00	82.00	83.64	85.00	87.14	88.75	90.00	91.00
120	W	72.02	77.49	82.80	86.93	90.24	92.94	95.20	98.74	101.60	105.70	108.90
	T	80.00	85.71	90.00	93.33	96.00	98.18	100.00	102.90	105.00	106.70	108.00
150	W	82.98	85.66	89.45	95.76	101.20	105.40	109.00	114.70	121.60	127.00	131.30
	T	90.00	98.57	105.00	110.00	114.00	117.30	120.00	124.30	127.50	130.00	132.00

2.5 Final Bridge Parameters

For this numerical study, the desired passable vehicle was selected to be the 137.8 ton HETS under a one-way caution crossing. As described in Section 1.3, the approach outlined in this report requires the calculation of the minimum level of longitudinal and shear reinforcement required for passage of the desired vehicle. This critical level of reinforcement is determined based on the capacity evaluation procedure, described in detail in Section 2.4. In addition to finding the critical level of longitudinal and shear reinforcement, analysis is performed on models with levels of reinforcement above and below the critical level of reinforcement, producing a gradient of responses. For this study, the sensitivity of changing the level of longitudinal and shear reinforcement was investigated by varying the level of reinforcement by +/-10% from the critical level of reinforcement required for passage of the HETS.

In varying the level of flexural reinforcement, the cross section shown in Figure 2.2 served as the basis of the model. The number and spacing of longitudinal reinforcement was held constant and only the area of the bars was varied to produce the different levels of reinforcement. Based on the capacity evaluation approach outlined in Section 2.4., the critical level of reinforcement for passage of the HETS was determined to require six 509 mm^2 bars, corresponding to a steel ratio of 0.362%. From this critical level of longitudinal reinforcement, a variation of +/-10% of the area of steel in the critical case was analyzed.

For determining the levels of shear reinforcement for this project, the size and type of stirrups were based on the representative structure in Section 2.1. Namely, 2 legs of 12mm diameter stirrups were considered, as seen in Figure 2.2. To vary the level of shear reinforcement, only the spacing of the stirrups was changed for analysis. Based on the capacity evaluation procedure of Section 2.4, a stirrup spacing of 200mm was determined to be the minimum required for passage of the HETS vehicle. Parametric variation of the level of shear reinforcement consisted of increasing and decreasing the spacing of the stirrups to create steel ratio equal to the critical level +/-10%. A summary of the parametric variation in longitudinal and shear reinforcement is found in Table 2.6.

Table 2.6: Final parameters for flexural and shear reinforcement levels

	Critical for HETS Passage	Critical +10%	Critical -10%
Flexural Reinforcement	6 - 509mm^2 bars ρ = 0.362%	6 - 622mm^2 bars ρ = 0.398%	6 - 565mm^2 bars ρ = 0.326%
Shear Reinforcement	12mm dia. stirrups (2 legs) @ 200 mm spacing ρ = 0.565%	12mm dia. stirrups (2 legs) @ 180 mm spacing ρ = 0.628%	12mm dia. stirrups (2 legs) @ 220 mm spacing ρ = 0.514%

In addition to varying the level of longitudinal and shear reinforcement, it is necessary to consider the effect of cracking on the flexural stiffness of the structure for dynamic analysis. In reinforced concrete, cracking is a direct result of the largest load imposed on a member. For bridges, cracking in the girder is due to the combination of static dead loads and vehicular live loads, thus cracking results from the largest load in the girder's load history. For this study, two different load histories are considered to understand the sensitivity of flexural stiffness to cracking in the dynamic model. The first case is based on the standard AASHTO design loads outlined in Section 2.2. For the 13.9 m span, the HS20-44 truck governs as the largest design load, as shown in Figure 2.5. The second cracked state considered is due to the California Permit Truck shown in Figure 2.6. For the simply supported 13.9 m span, at most three axles of this permit vehicle will load the structure.

CHAPTER 3: STATIC MODEL

3.1 Analytical Tools

Two different types of analytical tools were used for predicting the inelastic response of bridge structures to imposed static loadings. The first of these tools is a sectional approach in which can predict the moment versus curvature response at a section; this then provides the effective flexural (or bending) stiffness, EI, at any point over the length of a member. The second of these tools is continuum analysis which can predict the full response of concrete bridges including the influence of shear, the behavior near supports and in regions of damage, and the expected state of cracking over the length of the member. The difference between the two is illustrated in Figure 3.1, with the type of prediction by continuum analysis is shown at the top of Figure 3.1 figure and that by sectional analysis is shown at the bottom of Figure 3.1.

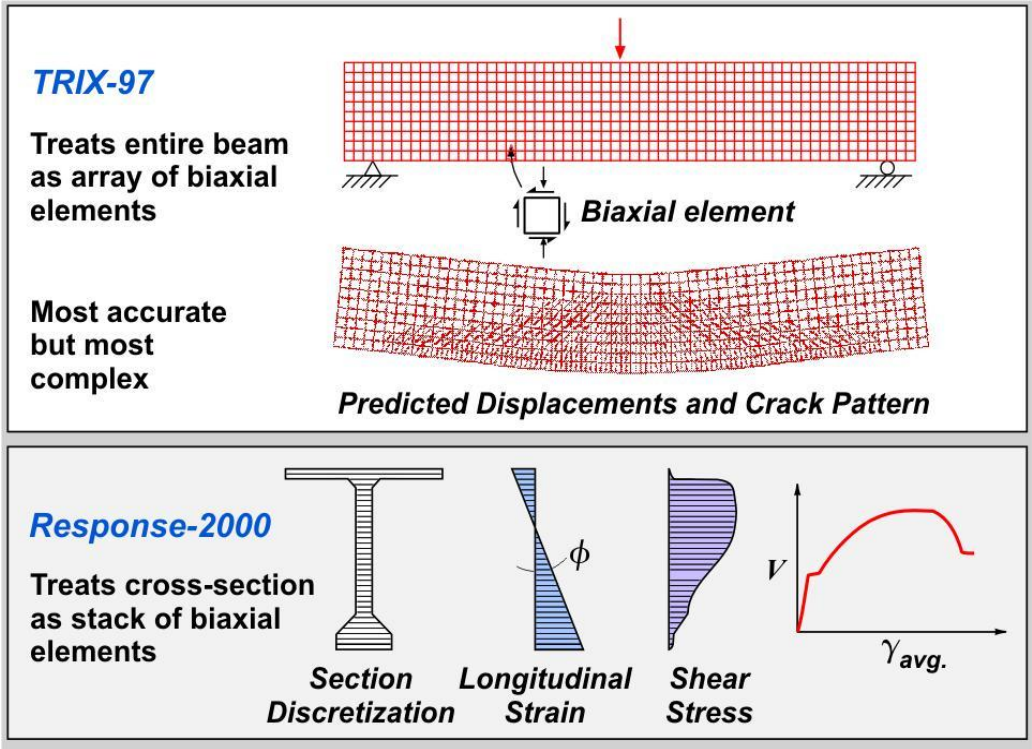

Figure 3.1: Illustration comparing continuum and sectional analysis tools (Vecchio & Collins, 1986)

3.1.1 Program Response-2000

Program Response-2000 is able to predict the complete moment versus curvature response of a section, which involves a multistep iterative process. At the lowest level, a multi-layer analysis methodology is used to evaluate the axial load and moment acting on a section for any strain gradient

over the height. This is done by calculating the state of stress in concrete and in the reinforcement at each individual layer over the height of a section using non-linear constitutive relationships and then employing equilibrium to determine the forces in each layer and thereby the forces (axial load and moment) acting on a section. There is one unique combination of axial load and moment for a single variation in longitudinal strain over the depth of the member. For a beam with no axial load, it is necessary to iterate on the curvature for any individual top strain to obtain one point on the moment-curvature response. Repeating this process for many levels of top strain provides a complete moment-curvature response for a section.

The geometry and material properties of a cross-section including reinforcement details can be readily input into Response-2000 using drop-down menus, typically a one minute process. The time required to complete a moment curvature analysis is similarly brief. The results of a sample analysis are shown in Figure 3.2. Each part of this figure will now be described in order to illustrate the depth of the information that is predicted from this type of analysis. The lower left image presents the calculated moment versus curvature response and above this is the moment versus longitudinal strain at the centroidal axis of the section.

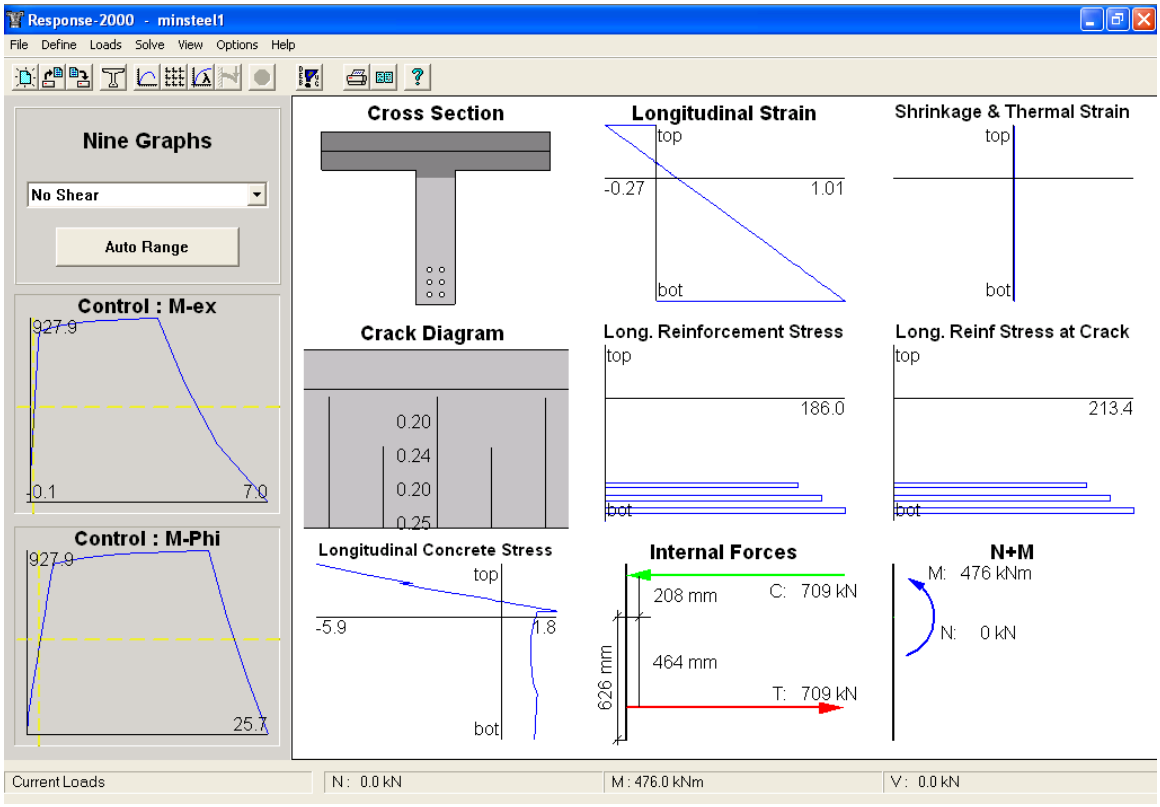

Figure 3.2: Response-2000 results output

Each of the other nine figures on the right present the condition of section for one particular level of moment. The information presented in each figures will now be described starting at the upper left image and then across its row before moving down to the next row. “Cross Section” presents the overall state of stress on an illustration of the cross-section. The shaded region represents the uncracked portion of the section while the unshaded region is the cracked portion of the section. The location of the reinforcement is also shown in this section and the color of the reinforcing bars is used to indicate yield and strain hardening. The next figure presents the profile of “Longitudinal Strain” over the depth of the member for the target axial load level (typically N=0 for a beam). The effect of “Shrinkage and Thermal Strains” can also be considered but in this example they were taken as zero. “Crack Diagram” presents the predicted depth and width of flexural cracking. The next two figures present the average stress in the “Longitudinal Reinforcement” and also that at a crack. The average stress is less than the stress at a crack due to the tension stiffening effect of the concrete that is still bonded to the reinforcement between cracks. “Longitudinal Concrete Stress” presents the concrete stress over the depth of the section based on the distribution of “Longitudinal Strain” that was presented in the top middle figure. As shown, the compressive stress is zero when the longitudinal strain is zero and then increases with compressive straining in a nonlinear manner. “Internal Forces” presents the centers of the compressive and tensile forces that are acting on the section and the distance between these forces. The axial load and moment acting on this section “N & M” can then be respectively calculated as the sum of these forces and the force coupling of these forces (Bentz, 2000).

3.1.2 Program VecTor2

VecTor2 is a nonlinear two-dimensional (2D) continuum finite element analysis (FEA) program for reinforced and prestressed concrete structures, formerly known as Trix-97, which employs the Modified Compression Field Theory (MCFT). The available materials in the program consist of reinforced concrete elements with or without smeared rebars and discrete rebars. It should be noted that the behavior models of MCFT are not bound with any specific constitutive relationship. Rather, they can be combined with any set of realistic constitutive relationships. Therefore, VecTor2 provides several choices of models for each material behavior. There is no specific guideline for the selection of constitutive models; the selection is completely up to users, which might result in the subjectivity of analytic result.

The element library of VecTor2 can be divided into three categories. First, for modeling reinforced concrete, planar triangular, rectangular and quadrilateral elements are available. The second category consists of linear truss element for discrete reinforcing bars. The third category is for bond-slip modeling between concrete and reinforcing bars, which has non-dimensional link and contact element.

Note that all elements are of linear order, which means the strain field within element is constant (Wong & Vecchio, 2002). Therefore, for the regions of complex stress distribution, a sufficiently fine mesh should be implemented to ensure quality results.

In order to solve the nonlinear problem, VecTor2 adopts secant stiffness solution method. This is possible because the strain-stress relationship of reinforced concrete is independent of loading history. During the iteration, the strain state is assumed first. Then, the assumption makes it possible to determine the corresponding constitutive relationship, from which the secant stiffness matrix becomes available immediately. The advantage of the method is that linear elastic finite element analysis program can be used without much modification.

The behavior of structural concrete is highly nonlinear in general, and thus it is usually the case that more than ten input parameters are needed for each material type in order to reproduce the complex behavior. Although VecTor2 also requires large amount of input parameters, since VecTor2 is a structural concrete analysis oriented program, it provides default values for most of material properties calculated from the basic set of measurable properties (e.g. f'_c , f_y , d_b of rebars, etc.) according to the relationships suggested by codes of practice or researchers.

A post-processor, Augustus, provides many options for viewing the predicted behavior. The output options include deformation, strains and stresses of reinforced concrete and discrete rebars, stress at crack surface, width and direction of crack, vital signs used for determination of health of structure, etc. Remembering that MCFT and VecTor2 are based on smeared crack concept, the locations and width of cracks represent average response of the structure, not real discrete local cracks.

In order to understand the predictive capability of VecTor2 it is necessary to understand the Modified Compression Field Theory (MCFT), which is the underlying behavioral model used in the program. The MCFT was proposed by Vecchio and Collins (1986). It was an extension of its predecessor, compression field theory (Mitchell & Collins, 1974). Later, the MCFT progressed to the new version of the theory, disturbed stress field model (DSFM) (Vecchio F. , 2000; Vecchio, Lai, Shim, & Ng, 2001; Vecchio F. , 2001). The MCFT and DSFM were implemented in nonlinear finite element analysis of reinforced concrete (NLFEARC) program, VecTor2, which was written and has been improved by Vecchio and his colleagues for two decades (Wong & Vecchio, 2002). Since the MCFT was not based on any specific constitutive relationships, this review does not include any specific constitutive relationships. For a more comprehensive review of MCFT and Vector2, see Collins and Mitchell (1991), ACI Committee 445 (1998), or Wong and Vecchio (2002).

The MCFT is an analytical model for the response of 2D membrane structures subjected to in-plane normal and shear stresses. The model accounts for the average stress-strain relationships in cracked concrete as well as perform an equilibrium check of conditions at crack locations.

The important assumptions of MCFT include:

1) The external normal and shear stress are uniform along the sides of an element.
2) The reinforced concrete element is independent of loading history, i.e. one strain state can have only one stress state.
3) For an element of which area spans a few cracks, average stress-strain relationship can be used. The tracks of individual cracks are not followed.
4) Rebars modeled as smeared rebar are perfectly bonded to surrounding concrete.
5) Rebars are uniformly distributed in an element.
6) Cracked concrete is an orthotropic material.
7) In cracked concrete, the direction of principal strains and stresses coincides with each other (this assumption was abandoned in DSFM).
8) The direction of crack is same as the direction of principal tensile strain.

Figure 3.3 shows the basic relationships of MCFT. The shear stress is applied to the membrane element. The external shear stress is resisted by the tensile stresses in the longitudinal reinforcement, f_{sx}, and the transverse reinforcement, f_{sy}, and a compressive stress, f_2, and a tensile stress, f_1, in the cracked concrete inclined at angle θ to the longitudinal axis. In the membrane elements of the figure, dashed lines indicate initial cracks, while solid lines represent the cracks developed later.

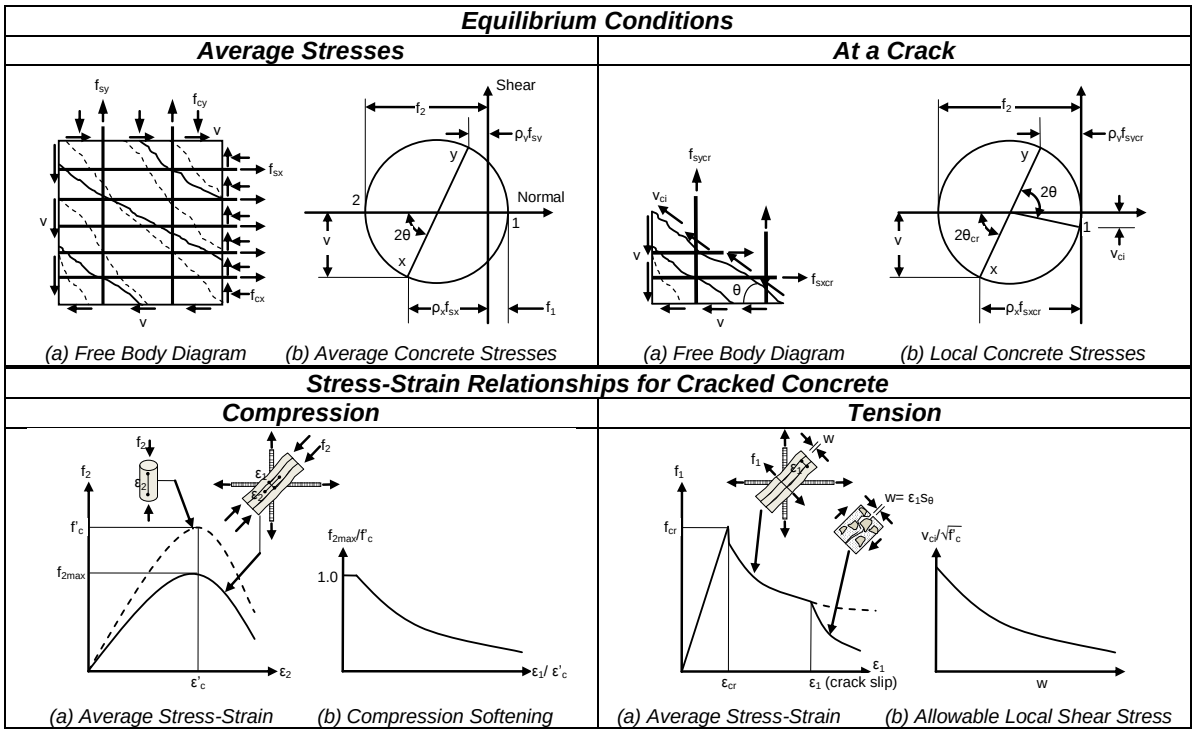

Figure 3.3: MFCT for membrane elements

The principal compressive stress in concrete, f_2, is resisted by the parallel chords of concrete called the compression field. The stress-strain relationship of the compression field is similar to that of uniaxial cylinder (dashed line in lower left graph), but the strength is reduced due to the existing transverse tensile strain (solid line), which is called compression softening. Typical relationship of compression softening is shown in the lower left of Figure 3.3.

In contrast to the tensile behavior of plain concrete where the tensile stress diminishes very fast after cracking, relatively heavily reinforced concrete shows much more ductile behavior. Stated differently, the tensile behavior of reinforcing bars surrounded by concrete is stiffer than the response of a bare bar. In order to account for the behavior of reinforced concrete element, tension stiffening relationship is used in MCFT, which is presented in the lower right part of Figure 3.3. By considering tension stiffening relationship with the stiffness of bare bar, the stiffer tensile response of the reinforced concrete can be modeled properly.

The principal tensile stress is resisted by the combination of reinforcement and tensile stress of concrete in terms of tension stiffening. However, at the crack surface, the stresses in the reinforcing bars increase in order to satisfy the equilibrium condition because the tensile stress of concrete almost reduces instantly. If the reinforcing bars have yielded and thus do not have sufficient strength to resist the tensile stress, shear stress develops at the crack surface in terms of aggregate interlocking. The capacity of shear stress reduces as the width of crack increases. Therefore, for large crack widths, the tensile capacity of concrete should be reduced in order to account for shear slip failure at crack surface. The crack width is calculated by the product of average tensile strain of concrete and average crack spacing, which is usually calculated based on the CEB-FIP model code 90 (CEB-FIB, 1993)

Besides the compressive and tensile behavior models described above, several behavior models have been added to the prototype of MCFT in order to improve the accuracy of analysis, e.g. Poisson effect, strength enhancement due to the confinement effect, tension softening.

Program Membrane-2000 utilizes the MCFT to analyze reinforced concrete membranes subjected to in-plane shear forces and axial loads (Bentz, 2000). Unlike VecTor2, which allows for analysis of a 2D continuum model comprised of multiple membrane elements, Membrane-2000 analyses a single membrane element, similar to the original derivation of the MCFT. For more information on Membrane-2000 and its capabilities, please refer to its user's manual (Bentz, 2001).

The MCFT was developed from and is validated by a large number of tests on reinforced concrete elements subjected to shear as well as combinations of shear and normal actions. An example of the predictive capability of the MCFT is presented in Figure 3.4 for four elements that contain a wide range in terms of levels of reinforcement.

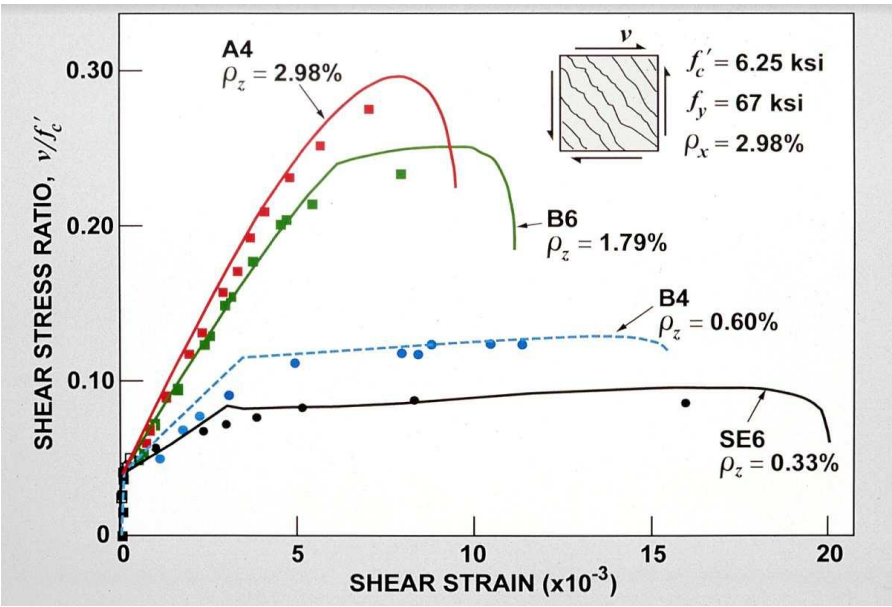

Figure 3.4: MCFT prediction versus results from shell membrane tests conducted at the University of Toronto (image courtesy of Michael Collins)

In keeping with general principles for the use of finite element methods, civil engineering structures can be considered to be composed of a large number of elements in which the behavior of each of these elements is dictated by the underlying principles of the MCFT. The types of structures whose behavior can be predicted well by the MCFT are shown in Figure 3.5.

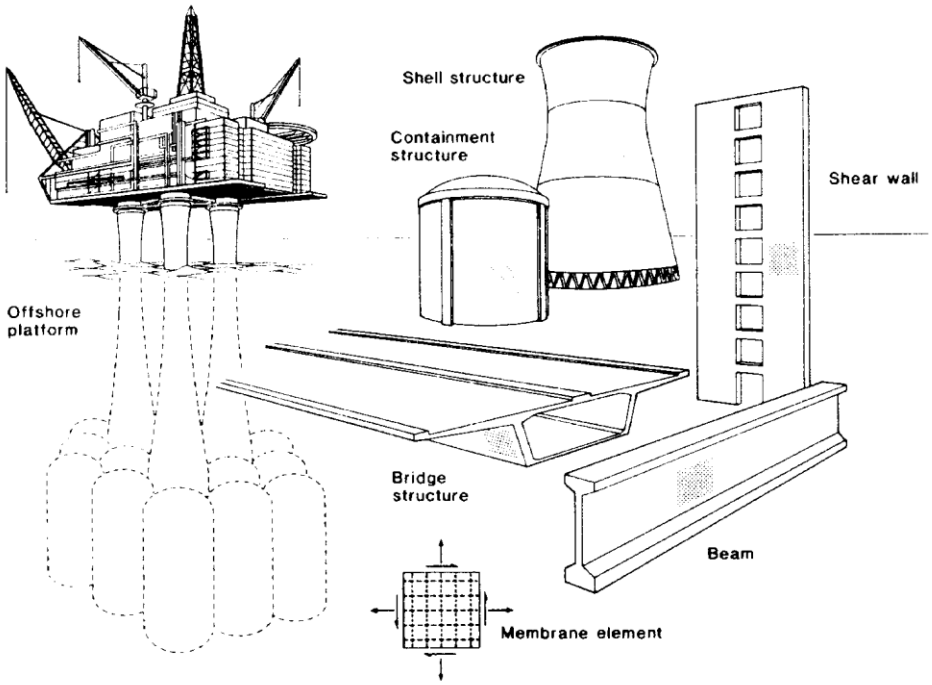

Figure 3.5: Structures idealized as an assemblage of membrane elements (Vecchio & Collins, 1986)

3.2 Models Used in Assessment

3.2.1 Continuum Model

The continuum model used in analysis was developed for the nonlinear finite element analysis program VecTor2, developed at the University of Toronto. The model is a two-dimensional model, with the member span and depth being the primary dimensions. The model was discretized into quadrilateral elements, with each quadrilateral element assigned a thickness corresponding to the thickness of the member at that location. By assigning appropriate thicknesses to the elements, the three dimensional structure is able to be accurately analyzed as a two-dimensional model as shown in Figure 3.6. Figure 3.6 illustrates the analyzed model for half of the span length; however, the entire span was modeled because the loads imposed on the structure were not symmetric about the midspan. Figure 3.7 illustrates the three-dimensional structure as rendered by the VecTor2 post-processing software, Augustus. This rendering serves to further demonstrate the capacity of representing the three-dimensional structure as a two-dimensional model for analysis.

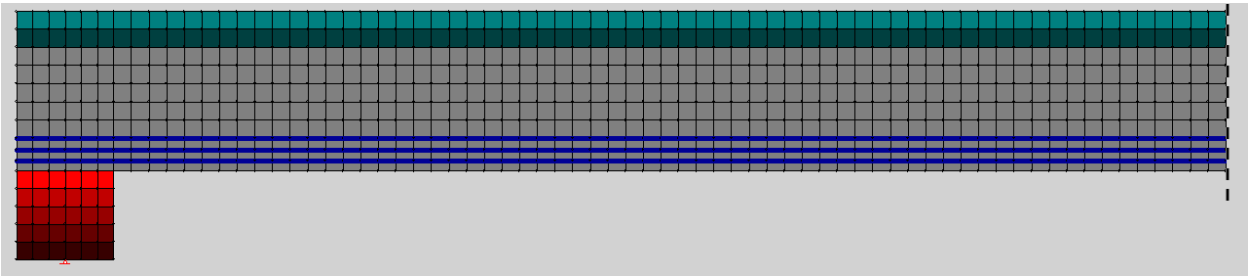

Figure 3.6: VecTor2 2D Continuum Finite Element Model

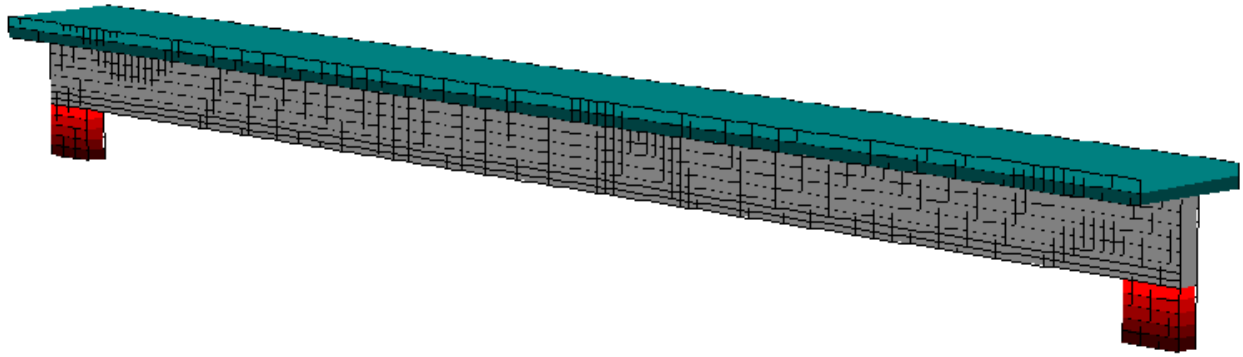

Figure 3.7: Three-Dimensional Rendering of Structure from VecTor2 Post-Processing

The quadrilateral elements used in analysis contain four nodes, each with two translational degrees of freedom. Based on experience with modeling in the program, the desirable element size for this structure was 60-120 mm. To capture the behavior of the vertical shear reinforcement, averaged, or smeared, reinforcement was assigned to the concrete elements. This reinforcement ratio for the vertical steel is dependent on the stirrup size and spacing as well as the thickness of the concrete element (web or flange). The longitudinal steel in the structure is modeled as discrete truss elements, as shown in blue in Figure 3.6. These truss elements connect between nodes at the corners of the quadrilateral elements and only resist elongation along their axis. Each truss element represents a layer of reinforcement with the area assigned to truss element equal to the sum of the areas of the individual bars associated with the layer of reinforcement.

In order to model the steel bearing pads without overly constraining the simply supported boundary conditions, the model supports, shown in red in Figure 3.6, are discretized into 5 horizontal layers. The bottom layer has the stiffness of steel, and each subsequent layer gradually decreases in stiffness until the stiffness of concrete at the bottom of the web. By modeling the supports this way, the model is not ineffectually constrained along the width of the bearing pad, which would induce unrealistic tensile stresses and cracking at the supports.

Loads were applied to the structure as equivalent nodal loads. A dead load was applied as a constant, uniformly distributed load along the span. Static live loads represent the tank axle loads for a given location of the tank. A distribution factor of 0.40 was used when considering the load carried to the analyzed girder. Static live loads were applied in increments of 2% of the full load until the full load was achieved. This incremental loading helps to ensure more accurate convergence of the nonlinear solver.

3.2.2 Sectional Models

Response-2000

The sectional model used in analysis was implemented in Response-2000, a fiber sectional analysis program developed at the University of Toronto. This program allows for user defined cross section geometry and allows for the user to assign different concrete properties to different regions of the cross section. Figure 3.8 shows the analyzed cross section for the critical level of steel. To accurately represent the structure described in Section 2.1, the top half of the flange is assigned a concrete compressive strength of 21 MPa, while the rest of the cross section is assigned a concrete compressive strength of 30 MPa. Layers of longitudinal reinforcement are assigned either as discrete numbers of bars at a given depth, or more generically as a total area of steel at a given depth. In this project, the variation of the level of longitudinal reinforcement was converted to an equivalent bar diameter corresponding to two bars at each level, in order to be consistent with cross section in Figure 2.2.

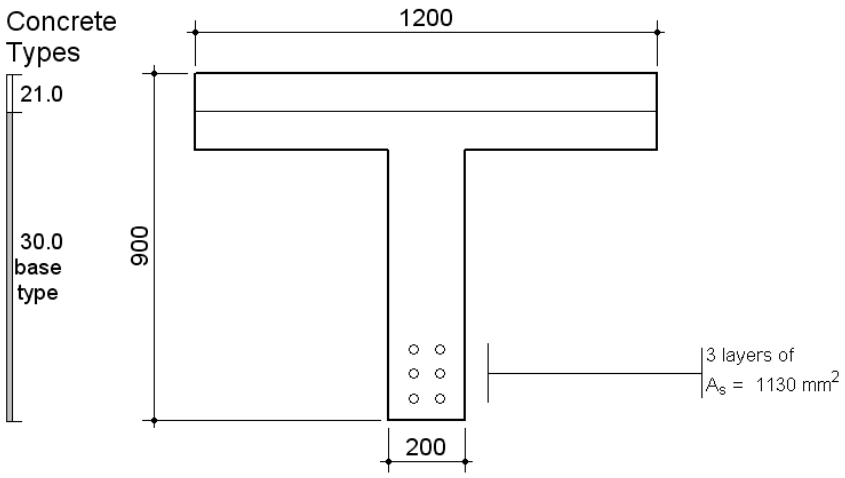

Figure 3.8: Section definition in Response2000

Membrane-2000

In addition to the Response2000 model, another sectional model was developed for use in investigating the shear response of the structure. Membrane-2000 is an analysis program for reinforced concrete membranes subjected to in-plane shear forces and axial loads (Bentz, 2000). Input into Membrane-2000 is similar to that of Response-2000, with user defined geometry (thickness), material properties, and reinforcement size and orientation. For analysis, the thickness of the membrane is specified to be equal to the thickness of the web of the girder. Reinforcement in the x-direction is held at a constant steel ratio of 1.5%, while y-direction reinforcement is specified to reflect the steel ratios associated with the different levels of shear reinforcement, as outline in Section 2.5.

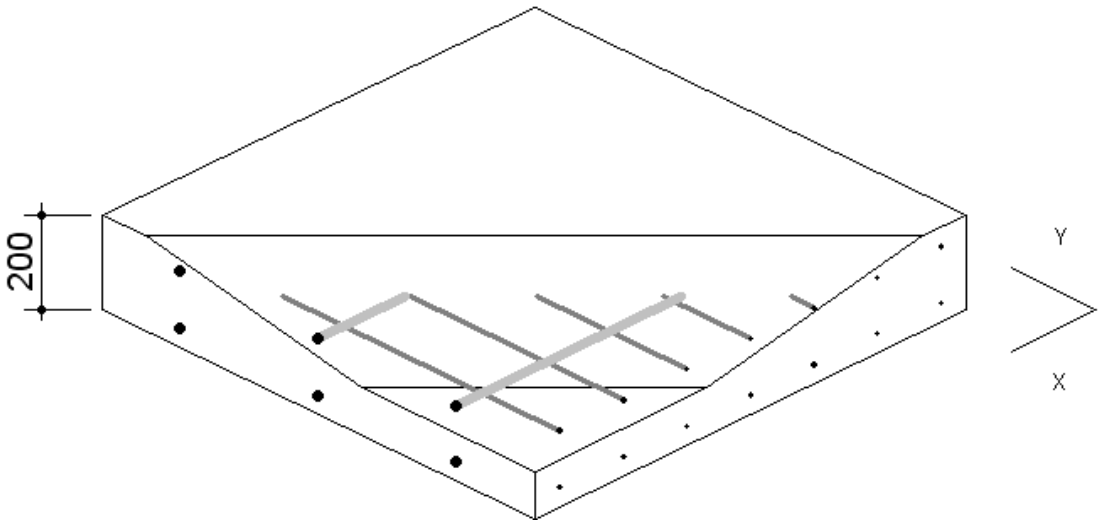

Figure 3.9: Sample membrane element from Membrane2000

3.3 Predicted Responses

3.3.1 Continuum Model

From the continuum model, it is possible to capture behavior along the length of the member. Element stresses and strains, crack patterns and distribution, and deflections can all be observed in post-processing. One response that is expected to be easily measured in the field is the deflection at the midspan of the structure under loading. Figure 3.10 shows the net deflection of the top of the structure under static tank loadings at different locations. The net deflection represents the measured deflection under live load, whereas the total deflection represents the deflection from the initially straight member due to dead and live loads. The tank location is based on the location of the center of the tank, thus when the tank location is at zero, axles on the front half of the tank are loading the structure and causing deflection at the midspan. The values from the analysis are tabulated in Table 3.1.

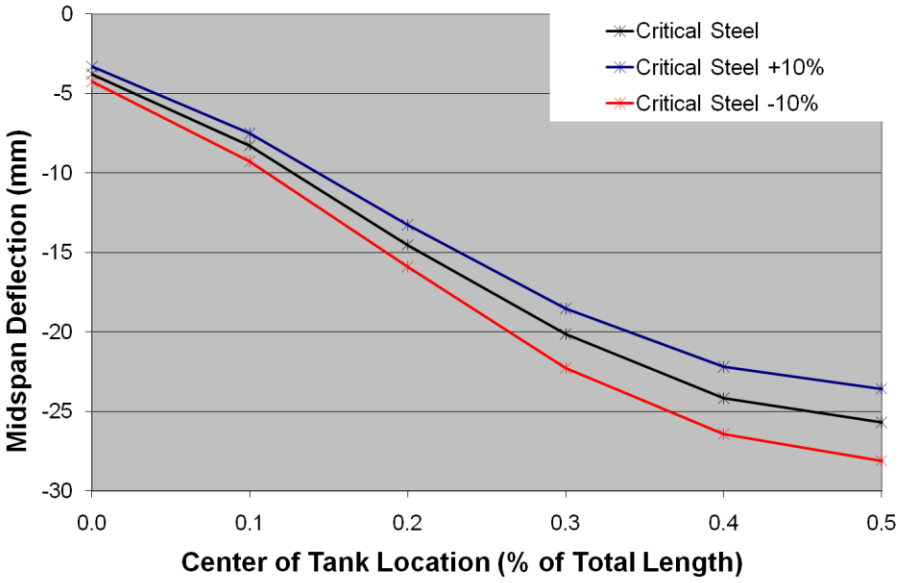

Figure 3.10: Net Midspan Displacement v. Tank Location

Table 3.1: Midspan Deflection v. Tank Location

	Midspan Deflection							
Level of Flexural Reinforcement	Critical Steel		Critical Steel +10%			Critical Steel -10%		
	Total (mm)	Net (mm)	Total (mm)	Net (mm)	Diff (%)*	Total (mm)	Net (mm)	Diff (%)*
Self Weight	-11.27	0.00	-10.45	0.00	0.00	-12.27	0.00	0.00
Tank @ L* 0.0	-15.04	-3.78	-13.75	-3.31	12.49%	-16.51	-4.24	-12.15%
Tank @ L* 0.1	-19.53	-8.27	-17.95	-7.50	9.26%	-21.55	-9.28	-12.26%
Tank @ L* 0.2	-25.78	-14.52	-23.70	-13.25	8.75%	-28.16	-15.89	-9.46%
Tank @ L* 0.3	-31.39	-20.12	-28.97	-18.52	7.96%	-34.55	-22.28	-10.69%
Tank @ L* 0.4	-35.43	-24.17	-32.64	-22.19	8.18%	-38.70	-26.43	-9.35%
Tank @ L* 0.5	-36.94	-25.68	-34.02	-23.57	8.21%	-40.36	-28.09	-9.41%

* Diff (%) represents the percent difference in net deflection from the critical steel condition

It is important to note that there is a clear separation of behavior between the different levels of reinforcement analyzed. For a 10% increase and decrease in the level of longitudinal reinforcement, the change in midspan deflection when the tank is located at the midspan is 8.2% and 9.4%, respectively. This difference can also be represented by an influence factor, which indicates the sensitivity of the measured response to changes in the level of longitudinal reinforcement. For this case, the influence factor for midspan deflection ranges between 0.82 and 0.94.

3.3.2 Sectional Model

Influence Lines

Sectional analysis provides useful information regarding behavior such as curvature and strain, which are governed by the flexural response of the structure. Looking at the response at a sectional level requires an understanding of the demand on the girder at a given point along its span. The use of influence lines are necessary to relate the loading on the entire structure to the demand imposed on a given point along one girder. Figure 3.11 shows two influence lines utilized in this study. Both influence lines in the figure represent the demand imposed at a single point of the girder, based on the uniformly distributed dead load and the location of the 80.5 ton M1-ABRAMS tank. The left figure represents the moment demand at midspan, while the image on the right represents the shear force at the left support. These influence lines are calculated by looking at the demand due to the axle loads at discrete locations along the member, accounting for distribution factor of 0.40. The black circles on the plot represent the relative spacing of the axles, meant to serve as relative scale reference with respect to the span.

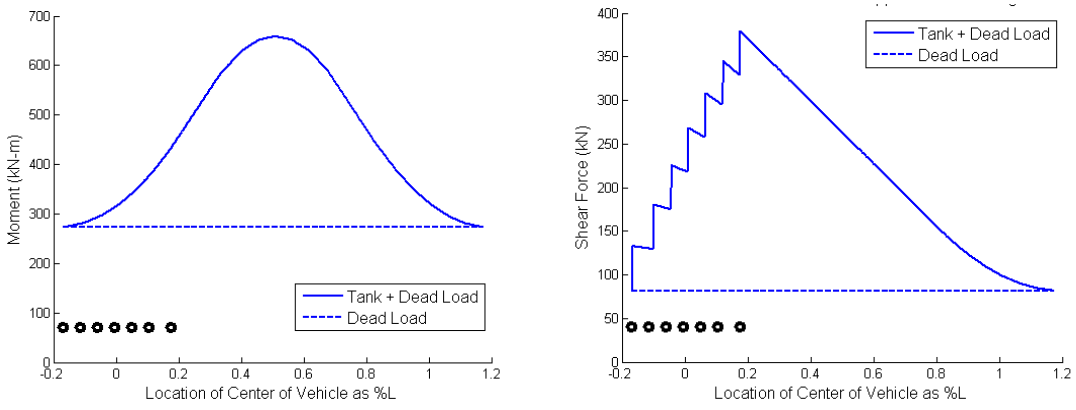

Figure 3.11: Tank influence lines for moving tank for midspan moment (left) and shear force at the left support (right)

It is important to remember that the analyzed girder is simply supported, thus any loading on adjacent spans have no influence on the analyzed girder. As such, the maximum midspan moment demand occurs when the tank is fully on the structure and located near the midspan of the structure. For shear, it is important to recognize the discontinuities in the influence line occur when a new axle enters the span. The maximum shear demand occurs when the last tank axle enters the span.

Flexural Response

Figure 3.12 shows the moment versus curvature results for the variation in longitudinal reinforcement. The response of each section is identical until the point of cracking, which occurs at a moment of 100 kN-m. After cracking, a clear delineation of behavior is present, with larger absolute differences in curvature at higher moment demands. Note that the plot represents the response of the structure under total demand, including dead and live loads. Due to self weight and superimposed dead loads, the girder is already subject to a load of 272.5 kN-m, as shown in the influence line in Figure 3.11. Thus, the structure is already expected to be cracked under self weight and any additional loading will elicit distinct structural response based on the level of flexural reinforcement.

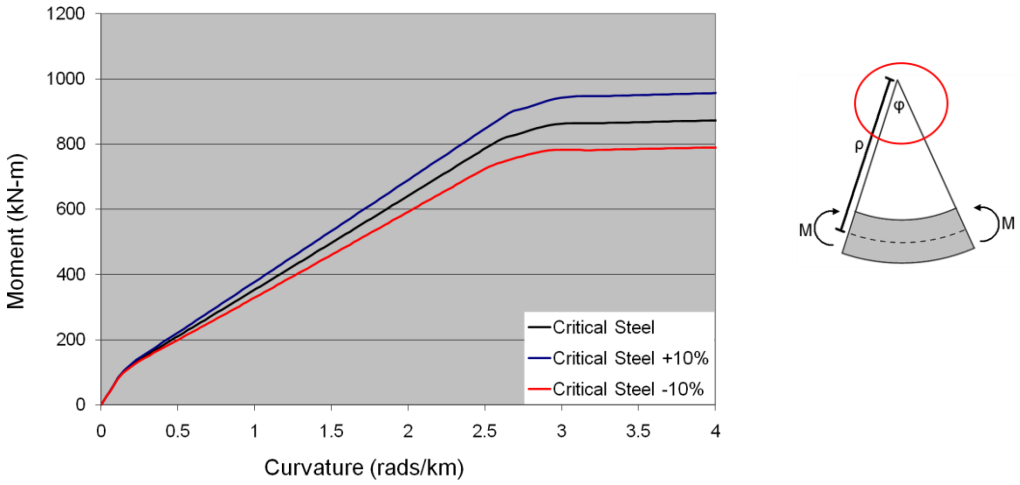

Figure 3.12: Moment v. Curvature

For Euler-Bernoulli beams, which do not consider shear deformations, the compressive and tensile strains of a beam can be calculated from the curvature and also can be read directly from Response-2000. Compressive and tensile strains are useful for field applications of this study due to their high potential in feasibility of accurate field measurements. The compressive strain behavior, shown in Figure 3.13, demonstrates clear separation of responses between the different levels of reinforcement. Compressive strain behavior is best measured at a discrete point, potentially through the use of a concrete

surface strain gage. The sensitivity of the instrumentation to capture these differences in behavior and feasibility of the approach is discussed further in Chapter 5.

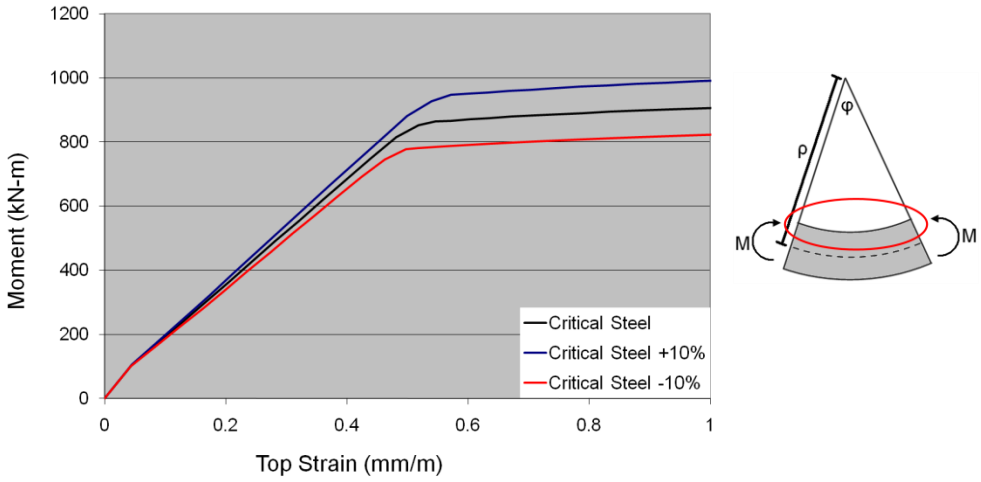

Figure 3.13: Moment v. Top Strain

Similarly, the tensile strain behavior is shown in Figure 3.14. The magnitude of the bottom strain after cracking is generally 2 - 5 times larger than the compressive strain at the same moment demand. It is important to recognize that the predicted tensile strain represents an average strain, which means that measurement of bottom strain needs to occur over a large enough domain to capture the average strain in the presence of flexural cracking.

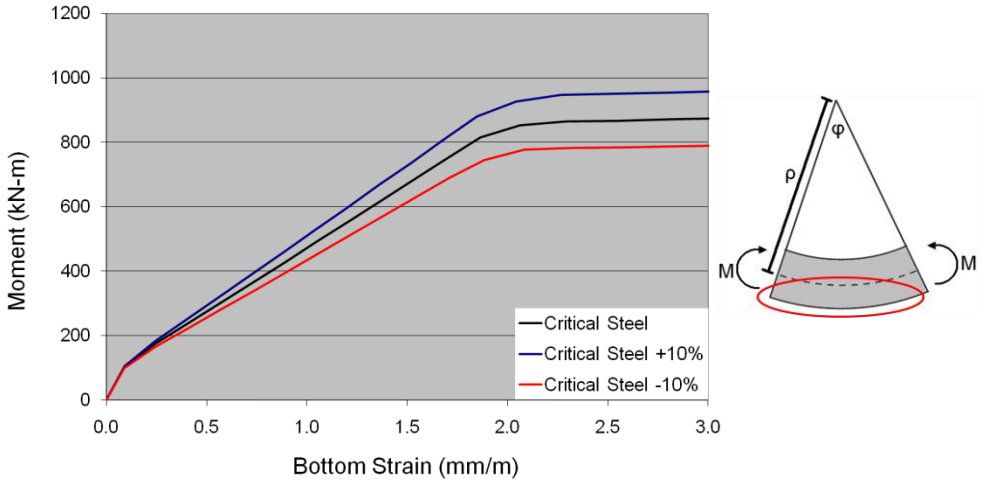

Figure 3.14: Moment v. Bottom Strain

Shear Response

From the Membrane2000 model, the shear response is comparatively analyzed for the different levels of shear reinforcement. Figure 3.15 shows the shear stress-strain plot for the parametric variation in vertical web reinforcement. Before cracking, at an average stress of 1.72 MPa and average strain of 0.07mm/m, all three elements exhibit identical behavior due to identical geometry and concrete properties. After initial loss of strength immediately after cracking, the elements gain shear strength from the transfer of force across cracks by the reinforcement, until the axial stress in the reinforcement reaches the yield stress of the steel. After cracking, each element exhibits a different response due to the different levels of shear reinforcement. As shown in Table 3.2, the post cracking shear strain of the elements are sensitive to the level of shear reinforcement by a influence factor of about 0.5. That is, for a given level of shear stress after cracking, the shear strain in the element varies by approximately 5% for a 10% change in the level of shear reinforcement.

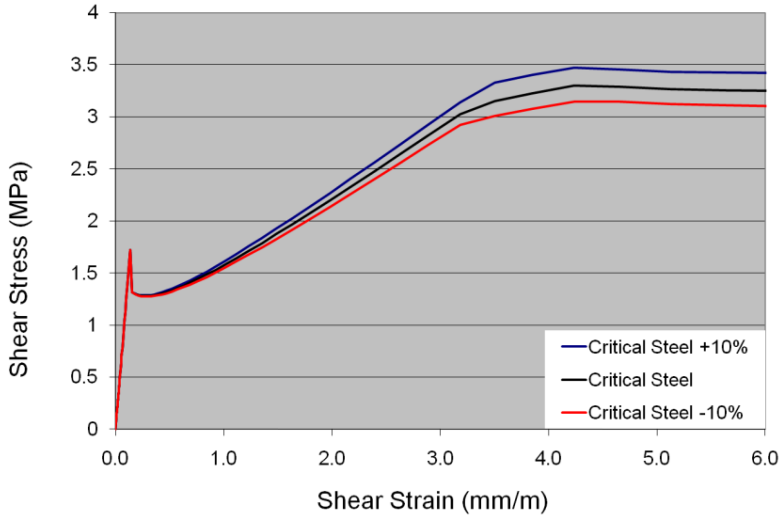

Figure 3.15: Shear Stress v. Shear Strain

Table 3.2: Shear Response Comparison of Sectional Models

Stress (MPa)	Critical Steel	Critical Steel +10%		Critical Steel -10%	
	Strain (mm/m)	Strain (mm/m)	% Change in Strain	Strain (mm/m)	% Change in Strain
1.5	0.867	0.817	5.70%	0.916	-5.70%
2	1.682	1.596	5.15%	1.765	-4.92%
2.5	2.426	2.304	5.01%	2.541	-4.77%

EI(x) for Dynamic Model Input

The flexural stiffness of the beam, EI(x), is required for input into the dynamic model. EI(x) is not constant along the length of a cracked reinforced concrete beam due to a varying moment of inertia, I, caused by the different extent of flexural cracking throughout the span. Typically, designers will use an effective moment of inertia, I_e, as a single value in calculating deflections and other serviceability considerations. Values of I_e are bound by the uncracked gross moment of inertia, I_g, and the cracked moment of inertia, I_{cr}. Different methods for determining I_e have been proposed and evaluated in research throughout the years. A discussion and review of some of the different approaches to determining the flexural rigidity of reinforced concrete beams is presented in Section 6.2.

In this project, the extent of cracking along the beam was considered by looking at the influence lines of two different vehicles, the HS20-44 AASHTO design vehicle and the California permit truck, as discussed in Section 2.2. The influence line utilized needed to represent the largest moment imposed at each point along the beam for the vehicle crossing the bridge. In other words, each point on the influence line represents the largest moment demand "felt" by the structure in its load history. For each point along the influence line, the curvature (φ) of the beam can be determined from the moment-curvature plot in Figure 3.12. From this information, the flexural stiffness at each point along the beam is evaluated by:

$$EI(x) = \frac{M(x)}{\varphi(x)}$$

Figure 3.16 demonstrates the calculation of EI(x) for the beam with the critical level of reinforcement with a HS20-44 load history. In the curvature plot, there is an evident abrupt change in behavior near the ends of the span, for example at x = 0.57m. This change in behavior demonstrates that the beam is not flexurally cracked for the first 57 cm from the support. This behavior is further demonstrated in the EI(x) plot, where in this region, EI(x) is equal to $EI_g(x)$, the flexural stiffness of the uncracked gross section.

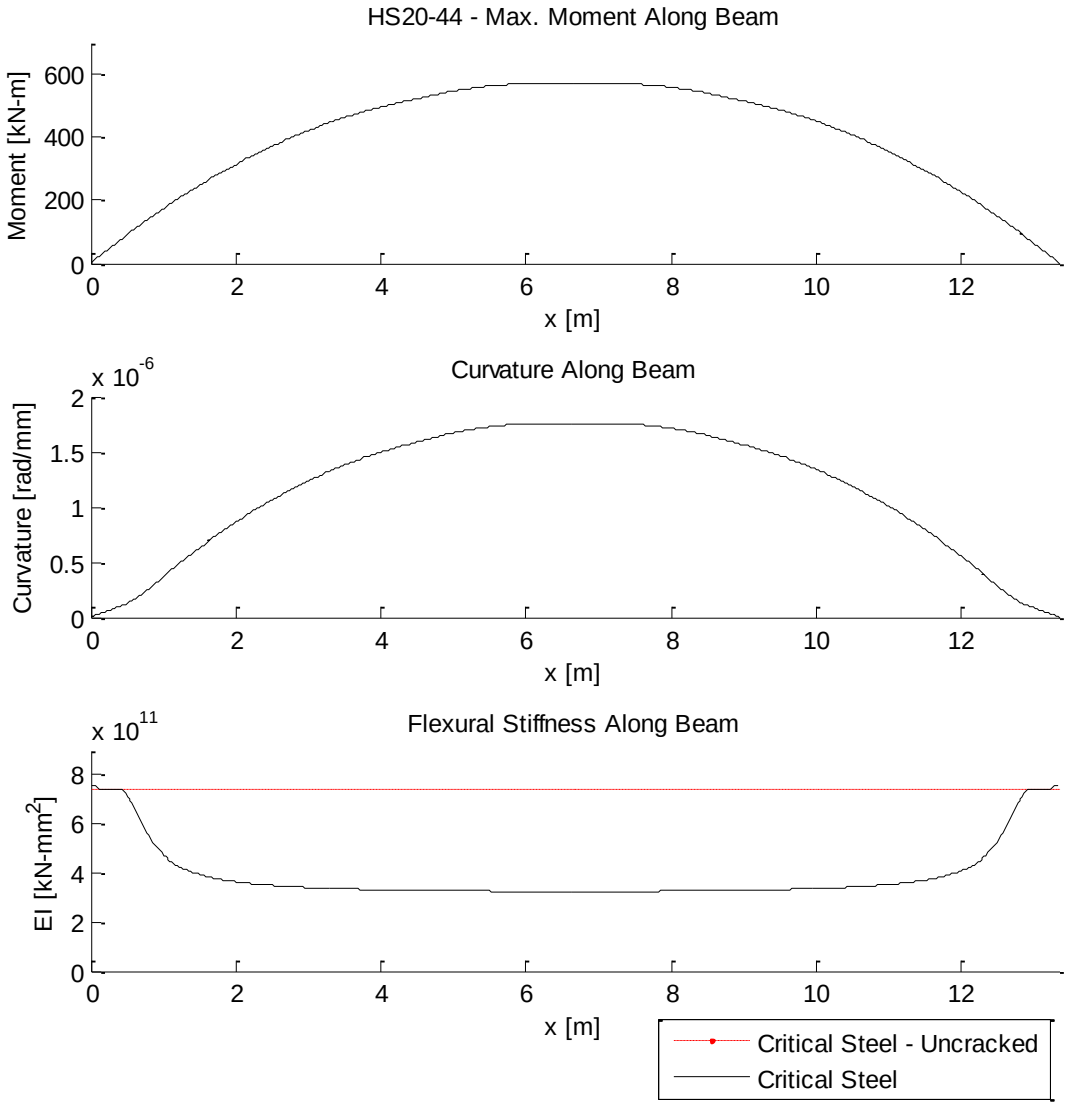

Figure 3.16: Derivation of EI(x) for critical level of longitudinal steel under HS20-44 load history

This procedure of calculating EI(x) along the beam was performed for the three levels of reinforcement under the two different load histories, as shown in Figure 3.17. As seen in the figure, the majority of the cracking in the beams is controlled primarily by the level of reinforcement rather than the load history.

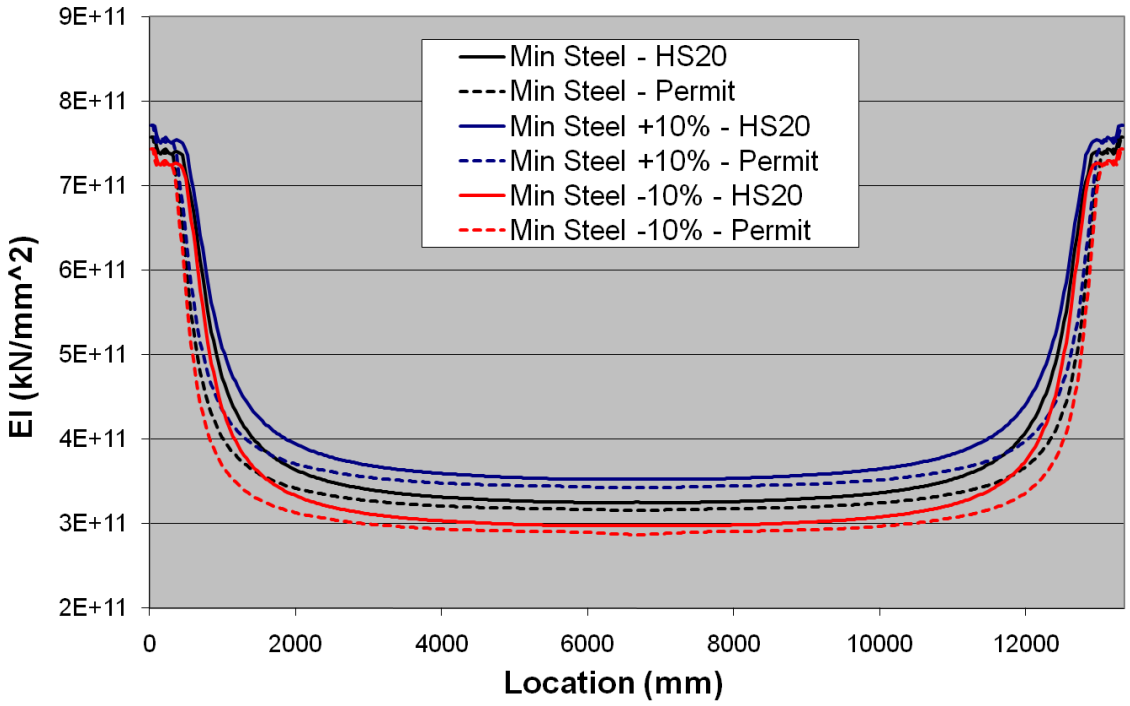

Figure 3.17: EI(x) for all different levels of reinforcement and load histories

CHAPTER 4: DYNAMIC MODEL

4.1 Models Used in Assessment

Measuring the dynamic response of the structure provides an additional means of assessing the level of longitudinal reinforcement in the girder. The level of longitudinal reinforcement affects the flexural stiffness of the girder and it is expected that girders with different levels of flexural reinforcement will exhibit distinctly different dynamic responses. The girders considered in this project are short, stiff structures which are less responsive to ambient excitation caused by lateral wind loads. In order to induce dynamic response, the model utilizes a vehicle crossing over a speed bump. The model, described in further detail in (Gries, Giles, Kuchma, Spencer, & Bergman, 2010) consists of a quarter car vehicle, the beam, and the speed bump (Figure 4.1).

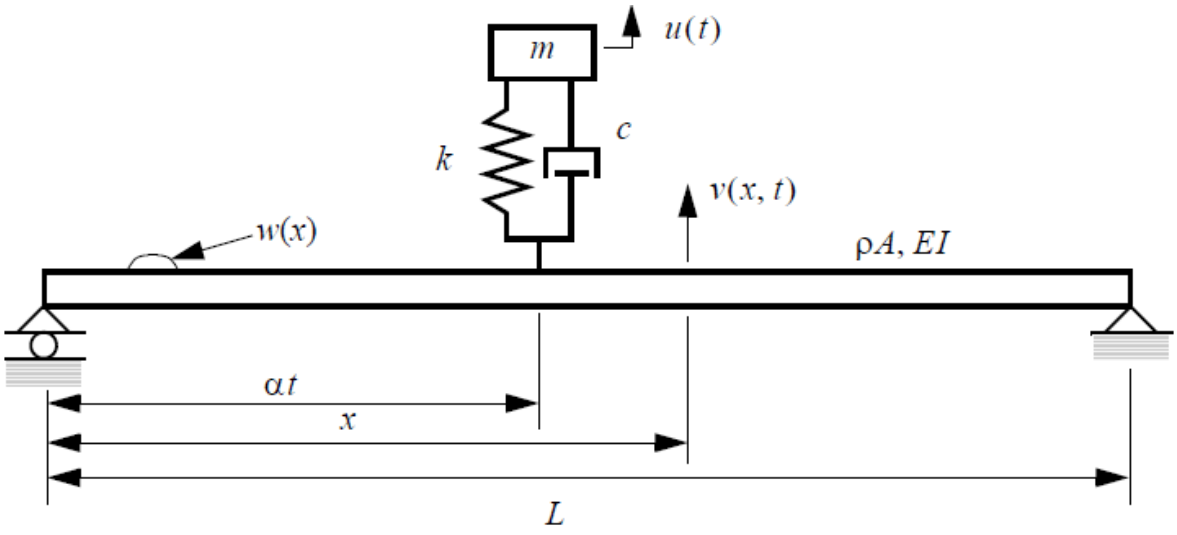

Figure 4.1:Diagram of a quarter car model on a beam with a bump

Vehicle Model

The vehicle is represented by a single axle, single degree of freedom quarter car model. The mass of the model represents half the axle weight of the vehicle while the stiffness and damping represent the net stiffness and damping of the vehicles suspension and tires. The vehicle's motion is interactive with and affected by the response of the bridge. The model could be expanded to incorporate more than one axle, but the quarter car model was chosen to simplify analysis in this preliminary numerical study.

Beam Model

The beam is modeled as a simply supported Euler-Bernoulli beam. The beams single degree of freedom is the transverse displacement, which is a function of time and the location of the vehicle. The

beam model utilizes an assumed modes approach for solution. Inputs into the beam model include the density and area of the gross section for the formulation of the mass matrix, EI(x) for the stiffness matrix, and a damping ratio for the damping matrix. The density of reinforced concrete is assumed to be 2450 kg/m^3 (150 lb/ft^3), and the area is found from the gross cross section. Rather that fitting a continuous curve to the data, EI(x) is input as discrete points along the beam with values from the calculations described in Section 3.3.2. A damping ratio of 4% was utilized and represents a typical value for reinforced concrete structures.

Speed Bump

The speed bump is a half-cosine shape with dimensions of 30 cm wide and 5 cm tall. These dimensions were selected so that the excitation is close to that of an impulse. An impulse excitation is ideal because it excites the entire frequency domain allowing for all the natural frequencies to be measured simultaneously (Gries, Giles, Kuchma, Spencer, & Bergman, 2010).

4.2 Predicted Responses

As previously mentioned, the variables that affect the flexural stiffness of the girders in the dynamic model are the level of flexural reinforcement and the cracked states, which are based on load history. The natural frequencies of the first three mode shapes of the girders are presented in Table 4.1 and Table 4.2. These tables demonstrate that the natural frequency increases in proportion to the level of longitudinal reinforcement for the same cracked state. The data consistently shows that a ten percent increase or decrease in the amount of longitudinal reinforcement produces a 4.1-4.3% change in the natural frequency for the same previous load history.

Table 4.1: Natural frequencies for girders with HS20-44 load history

	HS20-44 Truck				
Mode	Critical Steel	Critical Steel +10%		Critical Steel -10%	
	f_n (Hz)	f_n (Hz)	% Diff.	f_n (Hz)	% Diff.
1	5.34	5.56	4.12%	5.11	-4.31%
2	21.77	22.66	4.09%	20.83	-4.32%
3	49.58	51.60	4.07%	47.47	-4.26%

Table 4.2: Natural frequencies for girders with California permit load history

Mode	California Permit Truck				
	Critical Steel	Critical Steel +10%		Critical Steel -10%	
	f_n (Hz)	f_n (Hz)	% Diff.	f_n (Hz)	% Diff.
1	5.25	5.47	4.19%	5.02	-4.38%
2	21.29	22.17	4.13%	20.37	-4.32%
3	48.31	50.29	4.10%	46.21	-4.35%

In order to understand how the degree of flexural cracking affects the dynamic response, it is necessary to compare the response for both cracked states for the same level of reinforcement. Table 4.3 compares the natural frequencies for the critical level of steel reinforcement under both cracked states. From the table, it is evident that the natural frequency decreases as the level of cracking increases. The relative difference in natural frequency is less sensitive to the change in load history than it is to the level of longitudinal reinforcement. This observation is especially true in the first mode, which is expected to be the dominate mode in the response of the structure.

Table 4.3: Natural frequencies for girders with critical level of reinforcement and different load histories

Mode	Critical Level of Longitudinal Steel			
	HS20-44	CA Permit	Difference	
	f_n (Hz)	f_n (Hz)	Absolute	Relative
1	5.34	5.25	0.09	1.69%
2	21.77	21.29	0.48	2.20%
3	49.58	48.31	1.27	2.56%

In addition to the natural frequency, other behavior can be observed from the dynamic model. Maximum values of displacement, velocity, and acceleration at the midspan of the structure for excitation caused by a HMMWV passing a speed bump placed at the one-third the span length from the support is shown in Table 4.4 and Table 4.5. From the information presented in the tables, we see that the influence of a 10% change in reinforcement results in a 9.5 - 11.5% change in maximum displacement and velocity. Maximum acceleration appears to be even more sensitive to the level of reinforcement, however, the sensitivity is much more variable.

Table 4.4: Response at girder midspan to HMMWV excitation over bump at L/3 from the end of the bridge for HS20-44 load history

	HS20-44 Truck				
	Critical Steel	Critical Steel +10%		Critical Steel -10%	
	Value	Value	% Diff.	Value	% Diff.
Displacement (mm)	1.32	1.18	-10.61%	1.47	11.36%
Velocity (mm/s)	9.00	8.13	-9.67%	10.03	11.44%
Acceleration (mg)	23.92	21.22	-11.29%	28.14	17.64%

Table 4.5: Response at girder midspan to HMMWV excitation over bump at L/3 from the end of the bridge for California permit truck load history

	California Permit Truck				
	Critical Steel	Critical Steel +10%		Critical Steel -10%	
	Value	Value	% Diff.	Value	% Diff.
Displacement (mm)	1.38	1.24	-10.14%	1.52	10.14%
Velocity (mm/s)	9.37	8.46	-9.71%	10.44	11.42%
Acceleration (mg)	25.89	21.61	-16.53%	29.23	12.90%

CHAPTER 5: APPROACH EVALUATION

5.1 Sensor Technology Survey

The proposed assessment procedure requires that the sensor technology used to capture the in-field behavior is capable of making precise measurements and is feasible for implementation. It is not the aim of this study to make definitive statements on the use of available sensory technologies; this study focuses on the predictive behavior and assesses the sensitivity of the predicted behavior to changes in the level of reinforcement. However, it is useful to provide a survey of current technologies that have potential application to the field and to also offer insight into potentially useful sensor technologies that are either in development or do not currently exist. This section of the report provides a brief survey of some of the useful technologies that have application in static measurements in the field. In addition to the information presented in this section, other sensor technologies are useful for measuring dynamic response, including accelerometers, GPS sensors, tiltmeters, and an instrumented speed bump (Gries, Giles, Kuchma, Spencer, & Bergman, 2010).

5.1.1 Extensometers

An extensometer is a device for measuring the change in distance between two points. In the laboratory, the most common types of extensometers used are Linear Variable Displacement Transducers (LVDTs), linear potentiometers, and Cable Extension Transducers (CET). The accuracy of each of currently available systems ranges from 0.001 times the range of motion for the most common quality measurement devices to 0.0001 times the range of motion for the highest quality measurement devices. This means that if a device was selected that had a range of measurement of 10 inches and the maximum achievable accuracy could be 0.001 inches. This level of precision is more than sufficient for distinguishing between the behavior of beams with different levels of reinforcement by measuring midspan displacements and tensile strain to a precision as illustrated in Table 3.1 and Table 5.1: Example Static Response - Tensile Strain at Midspan.

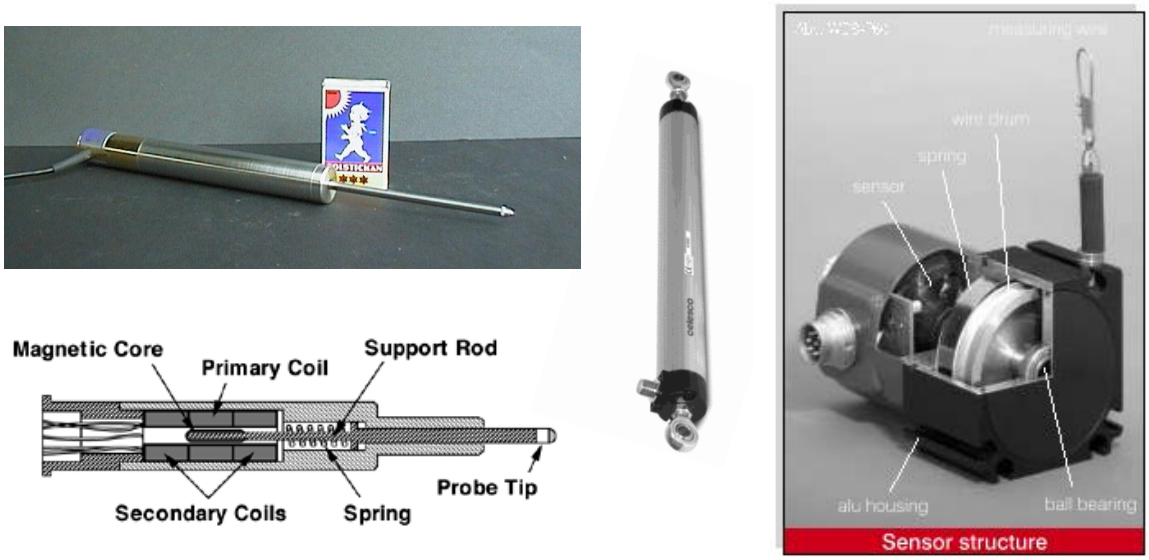

(a) LVDT (b) Potentiometer (c) CET

Figure 5.1: Types of displacement transducers used in structural testing laboratories

LVDTs and Potentiometers are likely the more suitable devices for measuring the changes in strain and curvature at selected locations on the surface of the bridge structure. Cable extension transducers are more suitable for measuring displacements from a datum for structures in the field. High-tension CETs have been used to measure displacements from datums of up to 150 feet. In their traditional use, all of these devices require wiring from a data acquisition system to provide sensor excitation and to make signal measurements. The time required to connect a few of these instruments by a well-trained team should be no more than a couple of hours provided that there is ready access to the girder from below the bridge structure.

5.1.2 Laser Trackers

Laser trackers provide one of the most promising technologies for being able to track the deflection and possibly the distribution of deflections and straining in bridge structures from a distance. These devices emit a pulsating laser beam to a mirrored target called a SMR (spherically mounted retro-reflector) (Figure 5.2, Figure 5.3).

By measuring the phase shift between a directly reflected pulse versus back which reflected off the SMR, the time of flight of the laser beam can be determined to about one billionth of a second. See Figure 5.4. This enables the distance to a distant object (perhaps 100 m) to be determined to an accuracy of a few millimeters.

Figure 5.2: SMR reflector

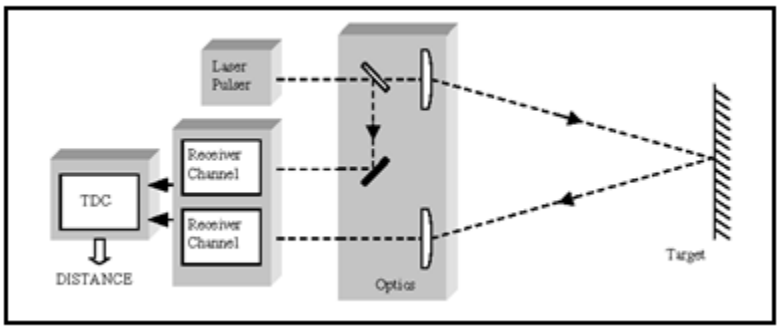

Figure 5.3: Flight path of laser beam

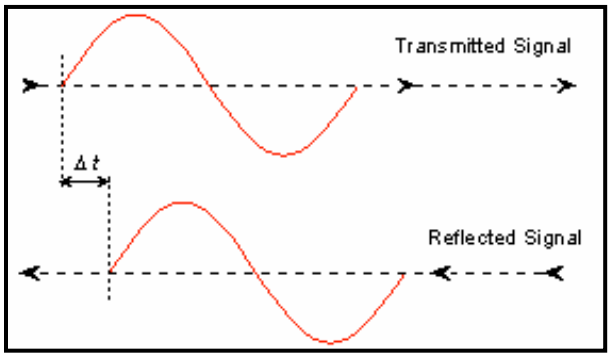

Figure 5.4: Phase shift in laser beam paths

This laser beam projects from an instrument that is able to measure the positional angle, both horizontal and vertical, to better than 1 arc second. Some manufacturers report being able to measure changes in angle to 0.25 arc seconds. More than 1000 readings per second can be measured by state-of-the-art devices such as those manufactured by Leica and Faro.

By setting the measurement instrument into tracking mode it is possible to use it to measure the downward movement at midspan of a bridge structure by mounting an SMR reflector on this bridge and then positioning the measurement instrument back a distance of up to a few hundred feet. In this way the accuracy of the measured displacement is directly proportional to the standoff distance. At a standoff distance of 100 feet, vertical displacements could be tracked to an accuracy of about 0.005 inches. At a standoff distance of 200 feet, vertical displacements could be tracked to an accuracy of about 0.01 inches. As seen in Figure 3.10, a 10% change in the quantity of reinforcement resulted in a difference in midspan deflection of more than 0.1 inches. Therefore, the accuracy for measuring vertical displacements using laser tracking systems is more than sufficient.

It is also possible to use laser tracker systems to track the changes in position of multiple SMRs. By measuring the change in distance between two SMRs it is possible to determine strains as well as

curvatures. For example, consider two SMRs located 100 inches apart at the bottom of a girder near midspan. If the measurement device was set back 100 feet from the bridge and a measurement accuracy of 1 arc second is assumed, then the strain can be determined to 50 micro strain. As presented in the example earlier in the report, this is just about the level of accuracy needed to distinguish a change in reinforcement amount of about 10%.

5.1.3 Photogrammetry

The last few years in metrology has seen the development of noncontact optical methods for measuring the shape, condition, and displacements of objects. All of the developed systems use long-standing photogrammetric principles for obtaining useful information from photographs. The affordability of high-resolution quality digital cameras and optics has spurred this development.

One example of how these methods are used is in Coordinate Measurement Machines (CMMs), which in this way they provide similar functionality as a laser tracker, but with certain advantages and disadvantages. The primary advantage in a field of operation is that it is not necessary to place a target, such as a SMR, on the bridge, rather, a natural marking on a girder can be used. The primary disadvantage is that significant post-processing of images can be required in order to assess displacements. Depending on the quality of the natural marker, errors can result in the post-processing. The accuracy of this system for making displacement measurements can be up to one ten-thousandths of the field of view in the image of the camera. Thereby, if the field of view within the image of the camera is 100 inches, then determining displacements to within about 0.01 inches is possible.

The number of cameras needed to make a measurement depends on the type of measurement to be made. If dimensional information is already available about the object, then it is possible to measure vector displacements with only one camera. If dimensional information is not available, then at least two cameras are needed and accuracy will increase with the number of cameras. Figure 5.5 illustrates how the position of multiple points on an object are recorded on the image space of the cameras Charged Coupling Device.

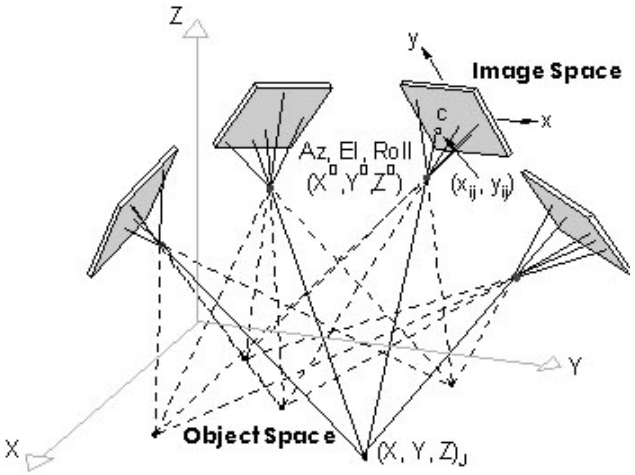

Figure 5.5: Photogrammetric method for coordinate measurement

Multiple camera setups have been used in structural laboratories to measure the displacements of a large number of points on the surface of the test girder as shown in Figure 5.6.

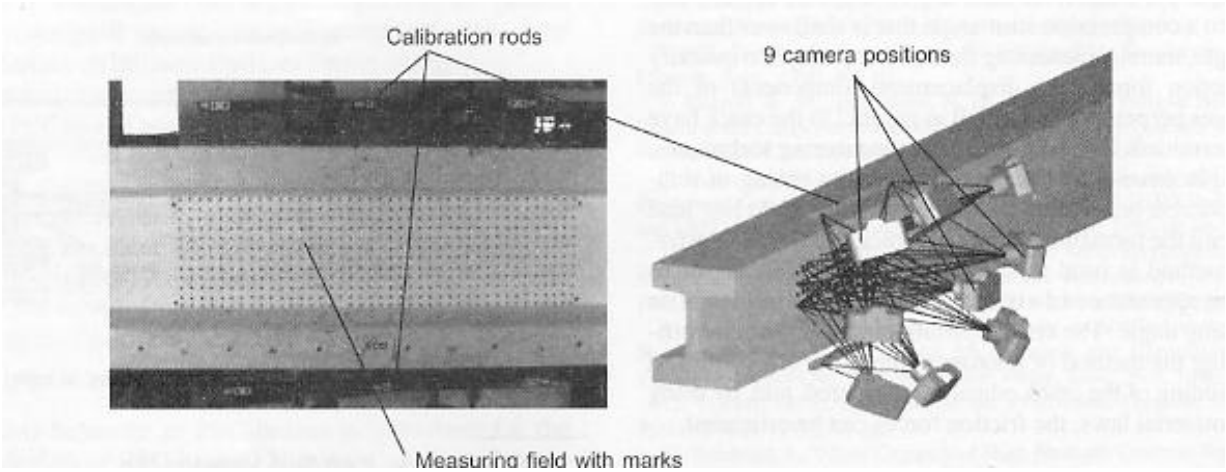

Figure 5.6: Method of photogrammetry for the study of the crack opening process of prestressed concrete beams (Hegger, 2004)

Photogrammetric methods can also be used for measuring the shapes of objects. Figure 5.7 illustrates how the shape and dimensions of a reinforced concrete wall were measured by taking pictures of this object with one camera from multiple positions. This may be particularly important for application in the field in which it is desired to obtain the dimensions of bridge components to a significant degree of accuracy.

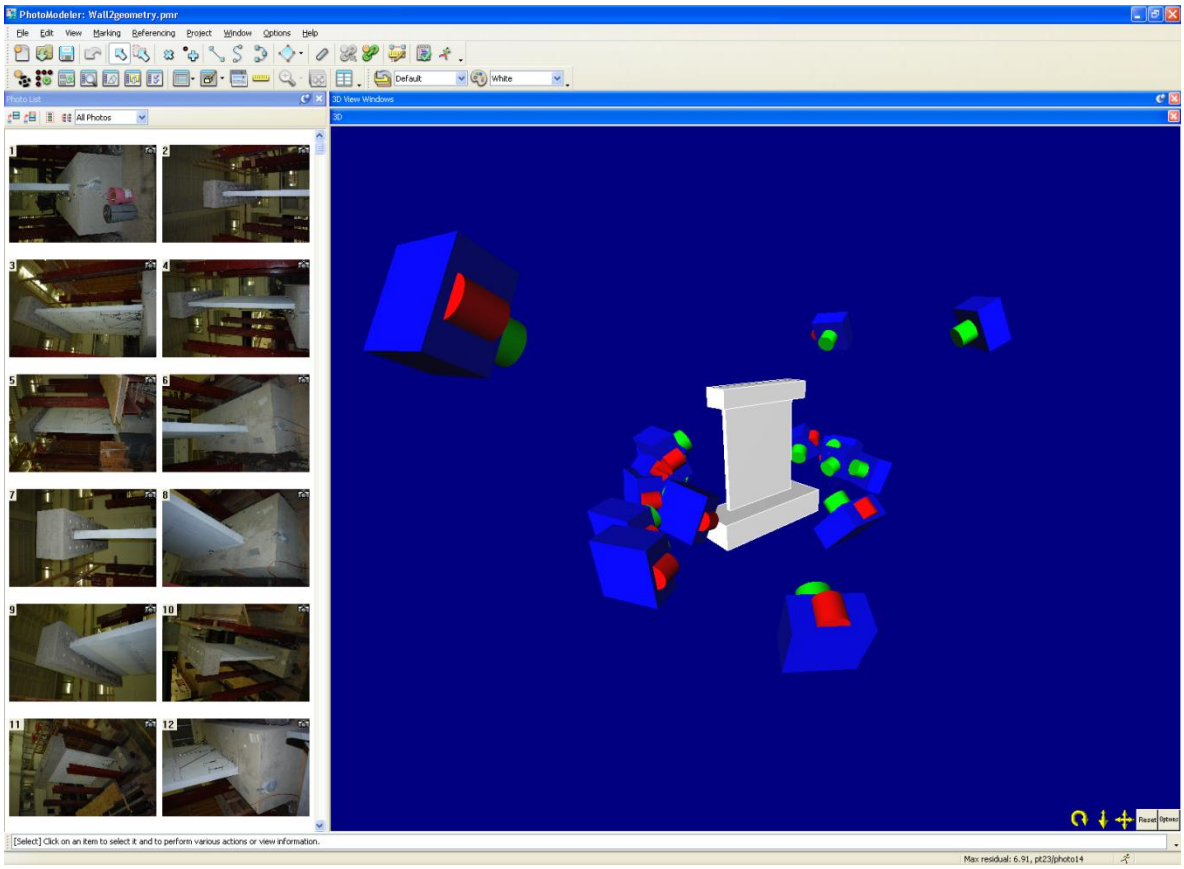

Figure 5.7: Measuring the shape of a concrete wall by photogrammetric methods

Photogrammetric and image analysis techniques have also been developed for identifying the locations of cracks on the surface of concrete structures as shown in Figure 5.8.

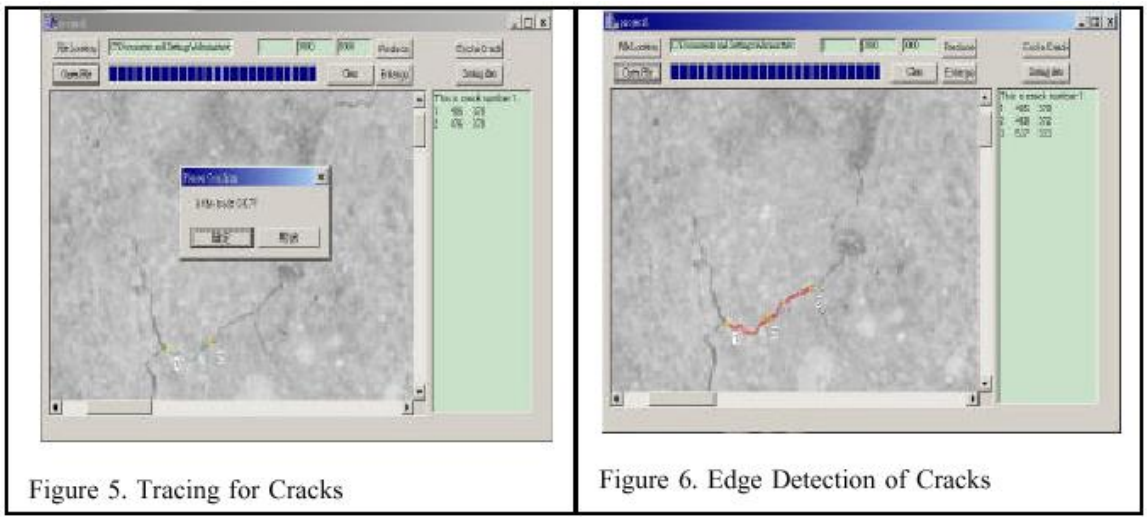

Figure 5.8: Crack detection by photogrammetric methods

This methodology was employed for developing complete crack maps for prestressed concrete girders that were tested at the University of Illinois as shown in Figure 5.9. If this type of information were available about members in the field, then it is possible that it could be used to identify both the level reinforcement in structures as well as the maximum loadings which that structure has seen.

(a) Girder in test setup

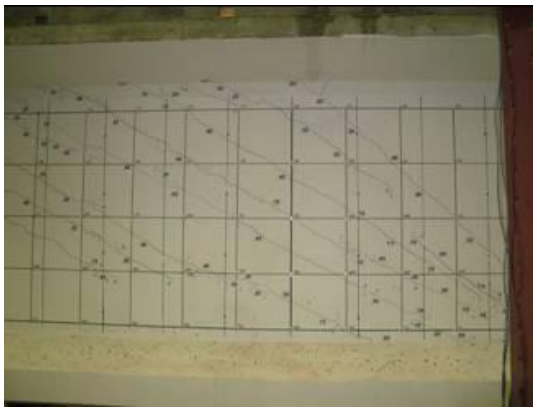

(b) Cracking captured by camera

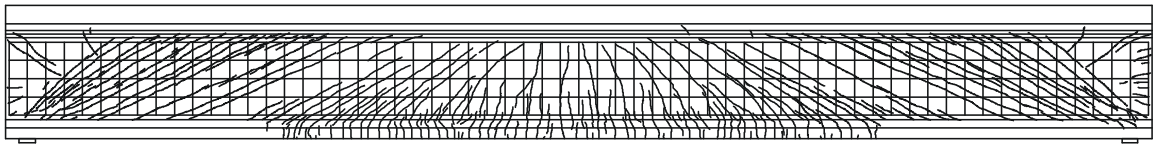

(c) Distribution of measured cracking over length of prestressed concrete test girder

Figure 5.9: The determination of crack patterns using photometric methods

5.1.4 Strain Gages

The strain gauge is the most commonly used device for measuring the response of structures to imposed loadings. Its strength is in the accuracy of its measurement which is typically in the range of one micro strain. This level of accuracy is not achieved by any other type of measuring device. However, there are several shortcomings as it pertains to the use of strain gauges to measure the response of reinforced concrete T-Beam bridges, including:

1) considerable effort is required to attach each gauge (approximately 1 hour per gauge)
2) wiring to a data-acquisition is required for excitation and signal measurement
3) strain gauges are quite small, and thereby their measurement only provides the condition at one point; this is particularly a problem for cracked concrete structures in which there is a wide range in response over a region such that the response of the region is more telling than the response at a point.

Despite the shortcomings, and particularly number (3), strain gauges can provide key information about the response of the member in flexure and in shear providing that informed selections of gage locations are made. An example of this is shown in Figure 5.10 below in which the numbered gauges 1-6 are being used to measure the magnitude of the compressive straining in the web of the prestressed concrete girder and gauges 7-9 are being used to assess the longitudinal demand placed on this girder from shear.

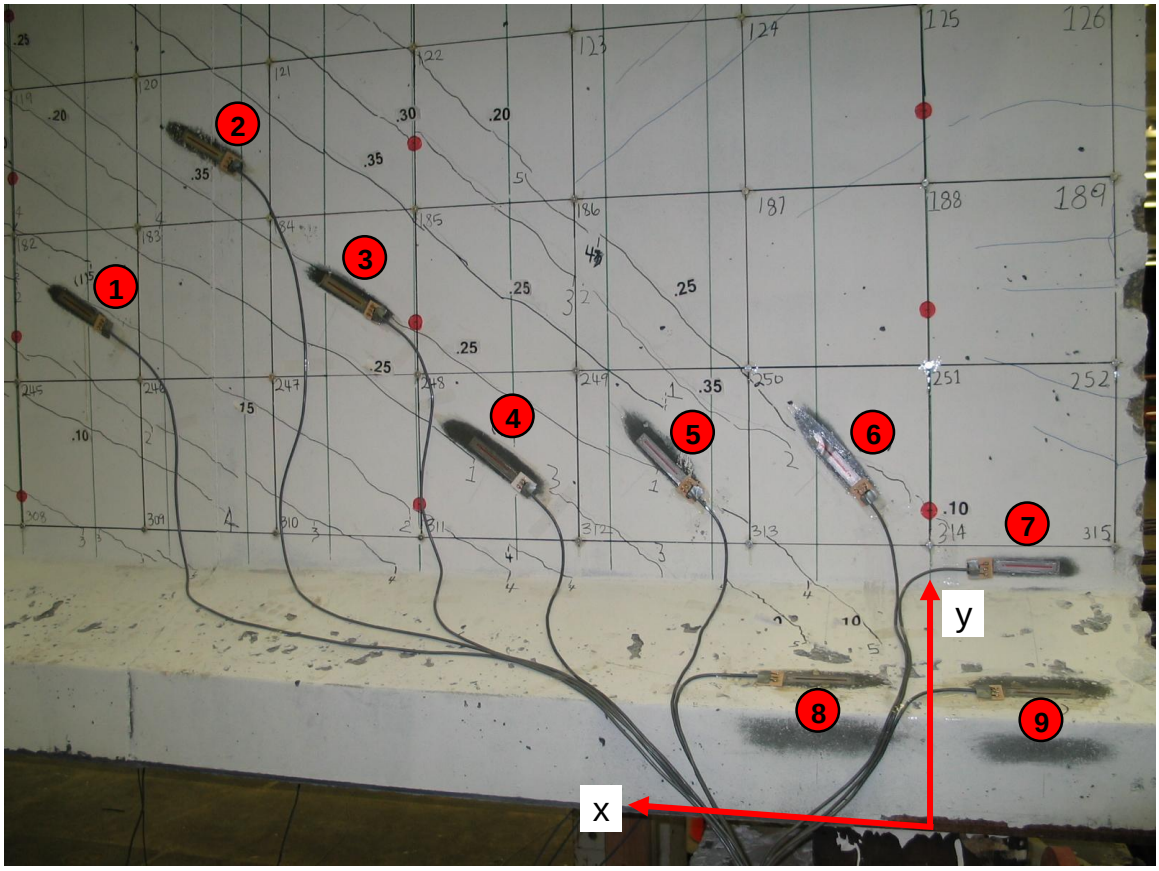

Figure 5.10: Concrete surface strain gauges on a prestressed concrete girder

5.2 Example Problem

5.2.1 Problem Description

In order to make the load carrying capacity assessment by the procedure outlined in Section 1.3, in-field measured response of the structure under known loads must be captured for comparison to the predicted response from nonlinear analysis. The assessment procedure outlined in this reports assumes that full access to the structure is possible to instrument the structure as necessary to capture response

under induced loading. In general, both dynamic and static loads are imposed on the structure for capturing the measured response. Dynamic excitation through induced vibrations can be performed by running a light military vehicle over a speed bump. A lighter military vehicle, such as a 3 ton HMMWV, is feasible for this test because relative differences in response due to different levels of reinforcement are not sensitive to scaling. That is, the percent difference between responses for different levels of reinforcement is not affected by overall magnitude of the response. For static loads, a heavier vehicle, such as the 80.5 ton M1-AMRAMS tank, is ideal for measuring static response such as displacements and strains. While the influence factor for a given static response for members with different levels of reinforcement is fairly consistent, the measurable differences of static response require a larger imposed load than the dynamic response. The following example illustrates one potential way to utilize dynamic and static tests to perform a capacity assessment. It is important to note that while the example details one type of measurement of both dynamic and static testing, increasing the number and types of measurements increases the confidence in the assessment.

Without advanced knowledge of the capacity of the structure, the procedure in this report anticipates that the dynamic testing would be performed first. In the dynamic test, the vehicle utilized is the HMMWV. Since this 3 ton vehicle is lighter than a typical highway design vehicle such as the 36 ton AASHTO HS20-44 truck, the effect of this vehicles weight and dynamic amplification if not expected to cause any damage concerns as it crosses the structure. In addition to safely crossing the structure, using a vehicle that is lighter than the expected vehicles in the load history of the structure is critical to ensure that the flexural stiffness input into the predictive analysis is not inaccurate due to further cracking during the dynamic test. To induce vibration with the vehicle, the test utilizes the dynamic speed bump described in Section 5.6. The first step to performing the dynamic test is to place the instrumented speed bump at the midspan of the girder, which requires that the speed bump be fully adhered to the surface of the deck. The hypothetical speed bump used in analysis in this report is a 5cm tall by 30 cm wide half-cosine. After the speed bump is securely adhered to the surface, the test vehicle moves over the structure at a velocity of 0.75 m/s (1.7 mph) and the data is captured by the instrumentation.

Once the dynamic test is complete, a first assessment on the level of reinforcement can be inferred. From this first dynamic assessment, it can be determined whether safe passage of the M1-ABRAMS tank can be expected for use in the static testing. If the results from the dynamic test indicate that the tank is safe for passage, the static load test can proceed. The instrumentation used in this example is designed to capture the average tensile strain on the bottom fiber at the midspan of the girder. Due to flexural cracking, the average tensile strain is determined from a measurement taken over a domain along the bottom fiber opposed to at a discrete point. For this reason, a strain gage cannot be used, but rather either an extensometer or targets for use with laser or photogrammetric means be adhered to the bottom

fiber at the midspan. After stopping the tank at midspan and waiting for any vibrations to diminish, the strain measurement is recorded.

5.2.2 Static Example Results

For the example described in Section 5.2.1, the measured strain reading from the instrumentation is compared to the predicted response gradient in Figure 3.14. In order to properly relate the information from the strain reading to the predictive response, it is critical to understand that the strain reading from in-field measurement only accounts for additional straining due to vehicular live loads. Therefore, the instrument strain reading is not the total strain as presented in the predicted response of Figure 3.14, but rather represents the difference in total strain from total load (dead plus live) and dead load only. Recall that the midspan moment demand under dead load and total load is read from the influence line shown in Figure 3.11. Figure 5.11 graphically represents the relation of the measured strain reading to the predicted response gradient. Additionally, the results are presented in Table 5.1.

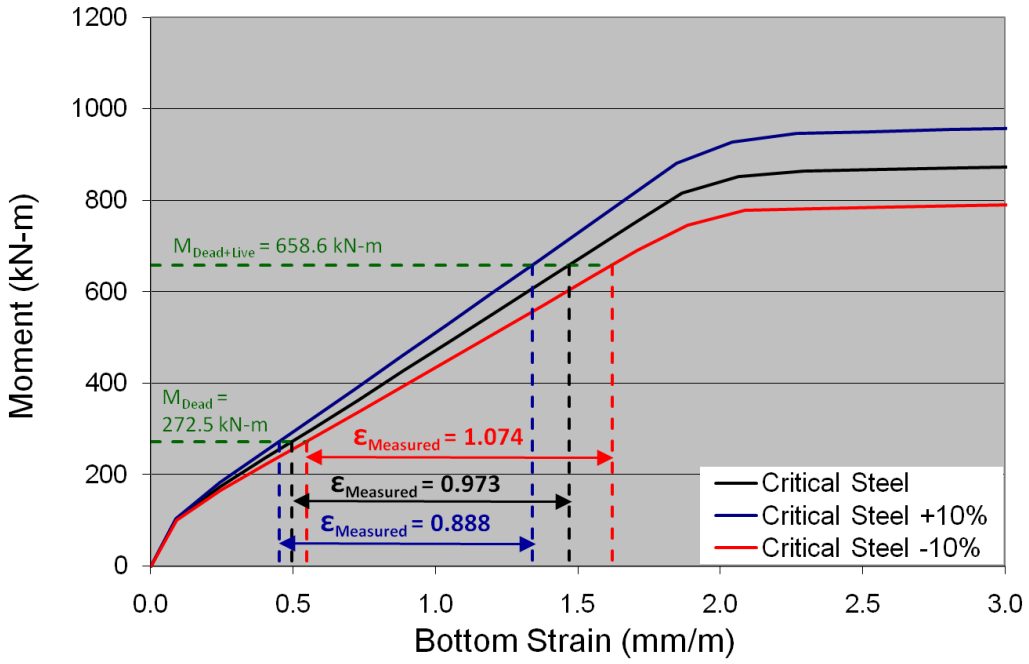

.

Figure 5.11: Interpretation of example static response

Table 5.1: Example Static Response - Tensile Strain at Midspan

Critical Steel		Critical Steel +10%			Critical Steel -10%		
Total Strain (mm/m)	Measured Strain (mm/m)	Total Strain (mm/m)	Measured Strain (mm/m)	Measured Strain Difference (%)	Total Strain (mm/m)	Measured Strain (mm/m)	Measured Strain Difference (%)
1.468	0.973	1.340	0.888	8.75%	1.622	1.074	-10.35%

From Table 5.1, it is clear that the measured tensile strain reading at midspan for the example test reflects the distinct behavior expected by the different levels of longitudinal reinforcement. As indicated in the table, the influence factor of level of longitudinal reinforcement on measured tensile strain is in the range of 0.85 to 1.05.

CHAPTER 6: LITERATURE REVIEW OF RELATED TOPICS

6.1 ERDC Multi-Resolution Approach

In a 2004 paper submitted to the ASCE Journal of Bridge Engineering, James Ray of the US Army Engineering Research and Development Center (ERDC) presented a methodology that seeks to provide rapid assessment of a large number of bridges and is applicable to any geographic region. The problem this paper sought to address was the U.S. military's need to make assessment of hundreds of bridges along convoy routes with little information on individual bridges. The approach utilizes a system of three discrete levels of assessment resolution (low, medium, and high resolutions) and employs a learning algorithm to improve low resolution assessments to medium resolution status. A description of the levels of assessment resolution follows.

Low resolution assessments are the first level of assessment and are performed on every bridge that needs to be assessed. Information regarding a bridge's location, route classification, and number and length of spans is gathered through aerial intelligence. The assessments that are able to be made at this resolution are based on correlations between design loads and military loads. Due to the very limited amount of information about the structure, low resolution assessments are less accurate and more conservative than the other assessments.

High resolution assessments are the most complete assessment level presented in the paper and are performed on a select number of structures. Through onsite inspection and obtaining complete structural dimensions, a thorough understanding of the structural makeup and condition of the bridge is obtained. From this information, a live load capacity assessment can be made, similar to the procedure outlined in Section 2.4 of this report. High resolution assessments are the most desirable, due to their high accuracy and low conservatism. However, when details of the structural components are not available or on-site inspection of the structure is not possible, a high resolution assessment cannot be evaluated.

Medium resolution assessments serve to provide less conservative and more accurate assessments than the low resolutions assessments for a bridge when a high resolution assessment is not possible. Medium resolution assessments are achieved by upgrading a low resolution assessment by process called machine learning. Machine learning identifies regional construction and condition tendencies from high resolution assessments. The adaptive algorithm in the machine learning process outlined in the paper determines bridge similarity based on span length, distance between bridges, and route type. Once similarity to a bridge which has undergone high resolution assessment is confirmed, a medium resolution assessment is established for the bridge.

This accuracy of the medium resolution assessments improve as more regional data is collected. The proposed methodology hinges on producing enough high resolution assessments, which require full understanding of the structural integrity of a bridge. The ERDC paper and proposed assessment methodology compliments the goals of this report. One potential application of the proposed in-field assessment procedure studied in this report is to help provide information regarding structural element details, namely the level of flexural and shear reinforcement, needed to make a high resolution assessment.

6.2 Flexural Rigidity, EI

One of the challenges of reinforced concrete design involves accurately predicting service load deflections of beams. As high strength concrete grew in popularity and the ACI code shifted to ultimate strength design in the mid 1960s, beams were designed to be much shallower and deflection under service loads became a concern (Wickline, Cousins, & Seda-Sanabria, 2003). In order to accurately predict deflections, it is necessary to accurately understand the flexural rigidity, EI, of the beam which requires thorough understanding of the moment of inertia, I. The moment of inertia varies along the length of the beam due to the different levels of cracking along the beam. Commonly, an effective moment of inertia, I_{eff}, simplifies calculations by serving as an average moment of inertia for the entire beam. The most commonly recognized and researched I_{eff} equation was developed by Branson in 1963 by looking at simply supported, uniformly loaded rectangular and T-beams. ACI Committee 435 presents this equation as (1966):

$$I_{eff} = \left(\frac{M_{cr}}{M}\right)^3 I_g + \left[1 - \left(\frac{M_{cr}}{M}\right)^3\right] I_{cr}$$

where

M_{cr} = cracking moment

M = maximum applied moment

I_g = moment of inertia of gross concrete section

I_{cr} = moment of inertia of cracked transformed section

This equation has been adopted by the ACI Building Code (2008) and is simple and inherently bound by the limits I_g and I_{cr}. However, experimental research indicates that the model is not consistently accurate to more than 20 percent of the lab measured deflections (Wickline, Cousins, & Seda-Sanabria, 2003).

In response to concern over the accuracy of Branson's model, other researchers have developed I_{eff} models, many of which are modified versions of the Branson model. The ERDC, through a project contracted to the Virginia Polytechnic Institute and State University, studied the effective moment of

inertia models for T-beam girders. In the report, T-beam girders with three different levels of reinforcement were subjected to tandem-axle load and measured deflections were compared to the response predicted by four different I_{eff} models. The first model studied, Branson's original model from 1963, consistently demonstrated large errors, with the largest errors associated with lower levels of reinforcement and lower applied moments.

Al-Zaid et al. presented two modified versions of the Branson model in 1991. The first model addressed the concern that load conditions other than uniformly distributed loads are not accurately captured in the Branson model. To address this concern, the exponent with the value of three is replaced in both cases with a general exponent, m. This general exponent is requires an experimentally measured moment of inertia to be evaluated. The other model presented by Al-Zaid et al. is based on the argument that one source of error in the original Branson model for beams with non-uniform load conditions is due to the various lengths over which a beam cracks under a specific load condition. Thus, a model based on the ratio of cracked and total length of the beam (I_{cr}/I), is used in lieu of the ratio M_{cr}/M. The cracked length form of the model also utilizes a general exponent, m. In both these cases, the accuracy of the model proved better than the original Branson model. However, the exponent m is a function of the level of reinforcement, thus its applicability to this project is limited.

The last effective moment of inertia model explored in the report was developed by Fikry and Thomas in 1998. Like the Al-Zaid models, the Fikry and Thomas model sought to account for non-uniform load configurations and variations in reinforcement (Wickline, Cousins, & Seda-Sanabria, 2003). One of the benefits of this model is that it does not require traditional calculation of I_{cr}, which can be burdensome. Rather, the formulation utilizes an approximate cracked moment of inertia which was found in the study to be within 6 percent of the actual cracked moment of inertia for all test specimens. In the study, however, the results from the Fikry and Thomas model were similar to that of the original Branson model (Wickline, Cousins, & Seda-Sanabria, 2003).

The results of the ERDC report on the accuracy of effective moment of inertia models proved largely inconclusive for application to the proposed assessment procedure presented in this report. The most accurate models from the study require a priori knowledge of the level of reinforcement in the girder, which makes its application to the proposed assessment procedure implausible. The models that do not rely on this information do not provide adequate precision in predicting the effective moment of inertia. For this preliminary sensitivity study, the flexural rigidity used in the dynamic model was based on calculating the curvature at discrete points along the beam, as described in Section 3.3.2. Curvature was determined based on sectional analysis for moment distribution from an influence line for the assumed largest vehicle in the bridges load history. It is expected that this method would underestimate the flexural rigidity of the beam because it ignores the tensile contribution of the concrete between cracks

(ACI Committee 435, 1966). The extent to which this method underestimates the flexural rigidity has not been determined in this report.

CHAPTER 7: CONCLUSIONS

7.1 Limitations

In order to place appropriate bounds on this preliminary numerical study to isolate key variables and identify areas of high potential for future research and development, there are a number of limitations that result from the underlying assumptions. These assumptions deal with the structure type and condition, material properties, distribution of load to girders, and the effects of different reinforcement detailing. This study made an earnest attempt to investigate the assumptions within the scope of the study, but further investigation into their effect on the findings of this report may require additional research and analysis.

Structure Type and Condition

The simply supported T-beam girder used in the analysis of this study was chosen based on discussions with the ERDC. As described in Section 2.1, this type of structure provides valuable insight into a class of commonly encountered bridges, regardless of geographic location. Analysis of a simply supported girder does not need to account for force transfer or interaction with adjacent spans due to the nature of the simply supported boundary conditions. When looking at the vehicular loads, only the axles that are on the span need to be considered. There exist other common classes of concrete bridges including reinforced concrete bridges with continuous girders across a support and prestressed structures. Identifying the class of structure requires visual inspection from a trained technician, and the class of structure changes the analytic approaches used in this study for determining the predicted response of the girder.

In addition to the type of structure, this project does not investigate the effects of damage to structural members or supports. Investigating the effects of damage is outside the scope of this project, however, further research including a full review of previous studies of bridge damage could prove constructive. Types of damage that may be useful include unseating of the girder from its bearing pad, damage due to impact or explosive hits like that described in Section 2.1, as well as the effects of corrosion.

Member Geometry

This report assumes that the member geometry, including dimensions of the gross cross section and span, is known. The degree to which the member geometry is known may be affected by the level of access to the structure. Speculation on how uncertainty in knowing the member dimensions affects results is not investigated in this report.

Material Properties

This report assumes that the compressive strength of the concrete (f'_c) and the yield strength of the reinforcing steel (f_y) are known. A parametric study was performed to verify that small (≤10%) variations of the properties of the materials would not affect results. This project assumes that the compressive strength of concrete can be accurately assessed from nondestructive means. This assumption requires full access to the structure. From analysis, the predicted response of the structure is not affected by a ±10% parametric variation of the stiffness and strength of concrete.

When looking at variations in the yield strength of the steel, the predicted behavior of the structure is not affected as long as the structure is not loaded to the point of yield in the reinforcement. The stiffness of reinforcing steel is constant for the types of steel used in reinforcement. Since post-yield steel behavior varies significantly between types of steel, predictability of any post-yield gains in strength from strain hardening is impossible in this type of assessment. This assessment does not allow for loads imposed on the structure to cause yielding in the reinforcement; thus as long as the estimate of yield strength is reasonably accurate and conservative, small variations in the steel strength will not affect results. Since there is not direct way to nondestructively test the yield strength of steel that is cast in concrete, yield strength may need to be predicted based on knowledge of regional construction practices.

Reinforcement Detailing

This project studied variations in the amount of reinforcement based on longitudinal bar size and vertical stirrup spacing, however, it does not investigate other possible reinforcement details. For example, older bridge structures may not utilize vertically oriented stirrups as the principle means of resisting shear. Rather, the use of bending the longitudinal bars at angles of 30º to 60º is common in many structures built in the early to mid 1900s. Additionally, this project looked at cases where the longitudinal reinforcement is placed continuously along the length of the member. The longitudinal reinforcement must be designed to resist the moment along the span, however, because the moment is usually largest near midspan, the reinforcement required near the ends of the girder is less than at midspan. For economy, the top layers of reinforcement may not run the entire span, but rather have cutoff locations to reduce the amount of steel in regions of lower moment demand.

Distribution of Load

This project assumes that the demand imposed on the analyzed girder is known. Calculation of dead and live load are known with high levels of confidence. Dead loads are calculated based on common densities of construction materials and known structure geometry. Live loads are known because the axle spacing and loads are known for the vehicles crossing the bridge. What is assumed in

this study is the distribution of these load demands to individual girders. In order to accurately predict the behavior of the girder under the procedure outlined in this report, it is necessary to know what percentage of the imposed loads is transferred to the measured girder. The distribution factors used in this report are based on AASHTO guidelines as well as practical experience. The precision of distribution factors continues to be an active area of research and the uncertainty associated with this assumption may warrant further investigation.

7.2 Future Work

The preliminary numerical study presented in this paper focused on assessing whether the amount of reinforcement in concrete bridges, and thereby load carrying capacity, could be determined from the measured response of these structures to static and/or dynamic loadings. The results of this study have illustrated that many different aspects of a bridge's response, including its deflections, curvatures, and frequencies, present distinctly different behavior that enable its load carrying capacity to be determined to within approximately 20%. These results constitute a significant improvement over current methods of in-field assessment which rely mainly on the external geometry of these structures for estimating capacity. This study has also revealed that, while conventional instrumentation technology is able to measure many important response characteristics, the use of emerging and/or the next generation of instrumentation technologies may greatly improve the ability to more quickly and accurately assess the load carrying capacity of bridge structures. This next generation of measurement capabilities is expected to be optically and laser-based.

This study was a purely analytical effort and made a number of assumptions, as described in Section 7.1. In order to further investigate the applicability of the proposed assessment procedure, further sensitivity analysis coupled with experimental validation is necessary. Anticipated steps for further research and development of the proposed capacity assessment procedure are:

1) Experimentally validate the accuracy of these analytical predictions by conducting physical static and dynamic tests on single girder bridge structures.
2) Identify what aspects of girder response provide the most useful indication of level of reinforcement, regardless if current technologies are sufficiently precise or implementable for the proposed assessment procedure. Develop new or improve existing technologies to meet needs.
3) Perform experimental assessment on a multi-girder structure to compare accuracy of predictive analysis and to further identify what improvements in analytical modeling and experimental measurement capabilities are needed to enable making sufficiently accurate

estimates of the load carrying capacity of a typical reinforced concrete bridge structure from its response to known imposed loadings.

4) Develop and validate a general procedure for assessing load carrying capacity of typical reinforced concrete bridges, including the development of software designed to streamline the procedure.

Brief discussion of these anticipated steps is presented in Sections 7.2.1-7.2.4.

7.2.1 Experimental Validation of Predictive Analysis - Single Girder Structure

Static Testing

A series of load tests will be conducted on simple-span single-girder reinforced concrete T-beams that are a reduced scale model of the T-beams of the selected bridge structure described throughout this report. These tests will be at a sufficiently large scale that regular deformed bar reinforcement and concrete may be used such that the results of the study will not be impaired by scale effects. It is expected that four different levels of flexural reinforcement and three different levels of shear reinforcement will be used in this study. Traditional instrumentation technologies will be used to measure the deflections, curvatures, slopes, and strains over the length of the structure. The measured response will be compared with the full analytical predictions to assess the accuracy and limitations of the numerical models. Load would be applied with actuators and the anticipated loading and measurement procedure would be:

1) Increase loading to first cracking
2) Mark cracks and record in photographs
3) Make other surface measurements
4) Unload to assess flexural stiffness
5) Repeat steps 1-4 , increasing the load from the previous largest load until failure is obtained after repeating the steps 10 or more times

Dynamic Testing

This evaluation will begin with tests on small-scale linear elastic physical models. These beams will be affixed with instrumented speed-bumps, and then the response of these structures to moving loads will be measured. This measured response will be compared with the predictions of numerical models to assess their accuracy and limitations. A setup for making similar types of evaluations has been used at the University of Illinois and is presented in Figure 7.1 (Biello, Bergman, & Kuchma, 2004).

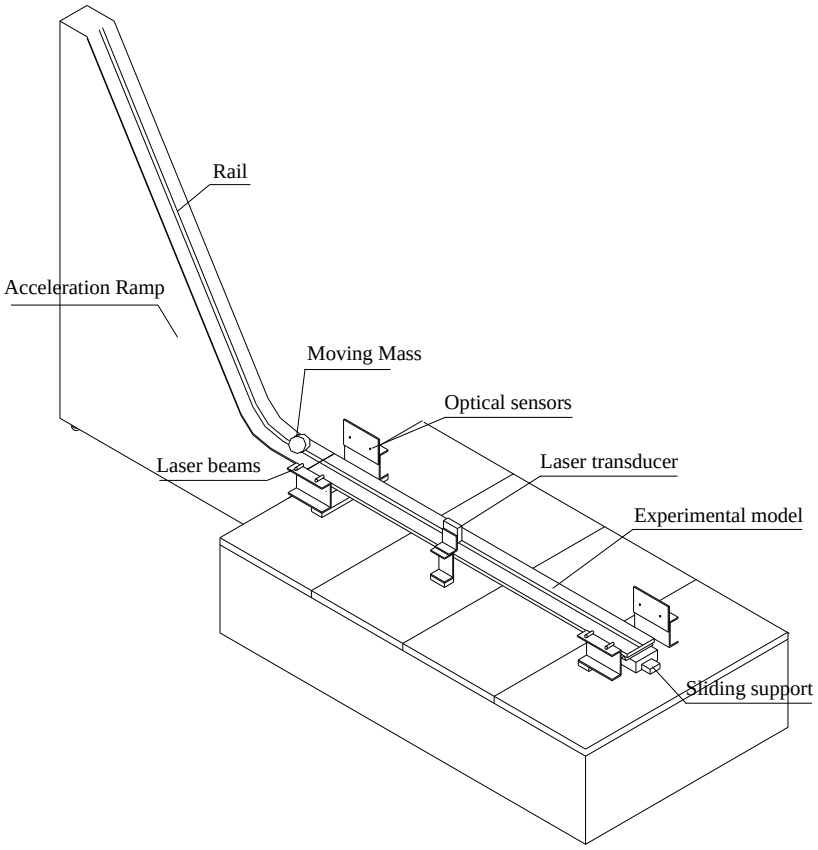

Figure 7.1: Proposed test setup for experimental verification of the dynamic predictive analysis (Biello, Bergman, & Kuchma, 2004)

In addition, the frequency of vibration of the reinforced concrete reduced-scale T-beams will also be measured at various levels of deformation and cracking over the loading history. This will provide an assessment as to how the dynamic response of these structures can be used to determine the extent of cracking and level of provided longitudinal reinforcement.

7.2.2 Sensor Technology Development

Throughout the experimental testing program, the research team will identify those aspects of beam response that provide important clues as to the reinforcing details, and thereby the load carrying capacity, and yet cannot be readily measured in the field using traditional instrumentation systems. Some of the critical aspects of response that may fall into this category are the distribution of cracking (spacing, width, depth, and angle), localized surface strains, and the distribution of flexural stiffness. From this information, assessment of available sensor technology can be further investigated and areas of potential sensor technology development can be identified.

One area of development that warrants further research is the development of an instrumented speed bump for use in dynamic testing. As described in Chapter 4, a vehicle driving over a bump serves as the source of dynamic excitation. By instrumenting this speed bump with an accelerometer and other potentially useful measurement tools, programmatic implementation in the field by trained technicians could be simplified. Successful implementation of this technology would require that the bump be securely adhered to the bridge deck and that instrumentation be securely fitted within the bump so as to ensure that measurements reflect the response of the structure.

7.2.3 Experimental Validation of Predictive Analysis – Multi-Girder Structure

Once the reliability of the predictive analysis procedures are assessed and verified through experimental testing of a single girder structure, verification of a multi-girder structure is necessary to continue developing the assessment procedure for field application. Testing of a multi-girder structure could either be performed on an existing bridge structure in collaboration with a governing agency such as the Illinois Department of Transportation or on a scaled structure built for controlled laboratory testing. If an existing structure is used, it is likely to be a relatively new structure so that the research team can obtain important properties that are often not known about the completed structure. Examples of these properties include measured material strengths, as built geometry, shrinkage strains, and bearing conditions. Assessment of the multi-girder structure offers an opportunity to make an assessment of missing elements and shortcomings of the numerical models, which may reflect some of the simplifying assumptions described in Section 7.1. Testing the multi-girder structure, whether in the controlled laboratory environment or on an existing full-scale structure, would require further investigation into distribution factors.

7.2.4 Procedure and Software Development

Once experimental testing has validated the predictive analysis techniques and measurement capabilities, a formal procedure and the required computational tools need to be developed. Depending on the application of the assessment procedure, the available time and access to the structure will limit the formal procedure. One of the assumptions of this preliminary numerical study indicates that time and access constraints are not yet considered. In order to implement the procedure, trained field technicians would require computational tools for data input and predictive analysis output. Ideally, these computational tools would consist of a portable computer with a clean, transparent user interface for input of member geometry, material strength, load conditions, etc. Predictive analysis could be performed directly on the computer or by sending the input information over the internet for analysis on another machine.

7.3 General Conclusions

The results presented in this report indicate that there is high potential for improving current methods of capacity assessment of reinforced concrete bridges through comparison of predictive analysis and measured behavior under known loads. This report represents the efforts from a preliminary numerical study designed to isolate key variables and identify areas of high potential for future research and development. Within the assumptions outlined in Section 7.1, the results are particularly promising for identifying the amount of flexural reinforcement in the structure. The flexural response, both displacement and strains, of girders with different levels of reinforcement exhibits both a consistent reinforcement influence factor as well as a discernable measureable difference with currently available sensor precision.

Shear response, on the other hand, presents a more difficult situation due to the very small magnitude of the response to shear, such as shear strain. As outlined in Section 2.3, common shear reinforcement design requirements have evolved and many bridges were constructed before minimum shear reinforcement requirements were introduced. Since shear failure is brittle in nature, it is dangerous to not have an accurate assessment of shear capacity when loading a structure with heavy loads such as an HETS tank carrier. Other possible solutions may need to be explored if further development of the shear assessment approaches in this study prove inadequate in the experimental validation tests. One possible solution, if the level of access permits, is to locate the location of shear reinforcement through the use of ground penetrating radar (GPR). GPR is currently used in construction practices to locate reinforcement before drilling into a reinforced concrete structure. In laboratory tests, GPR has not yet proven capable of identifying the diameter of reinforcement to an adequate accuracy for application to this project; however, it has shown promise in locating reinforcement (Zhan & Xie, 2009; Chang, Lin, & Lien, 2009; He, Zhu, Liu, & Lu, 2009). By using GPR to locate vertical stirrup spacing, a conservative assumption on stirrup diameter (#3 bars) and number of legs (2) could be made to more safely and accurately assess the shear capacity of the structure in lieu of measuring shear response under controlled loading.

It is important to understand that data obtained from field measurement is never going to result in the same consistently clear results from predictive analysis. As understanding of the load distributed to an individual girder and reliability of sensor technologies are improved, confidence in the measured behavior will increase. Measurement of the response of the structure should include recording a variety of different behaviors (strains, displacements, vibrations), performing different types of tests (static and dynamic), and repetition of each test. By obtaining data for different tests, statistical correlations can increase confidence in the capacity assessment made from the procedure.

REFERENCES

AASHTO. (1994). *American Association of State Highway Transportation Officials Manual for Condition Evaluation of Bridges* (2nd ed.). Washington, D.C.

ACI Committee 318. (2008). *Building Code Requirements for Structural Concrete (ACI 318-08) and Commentary.* American Concrete Institute,.

ACI Committee 435. (1966, June). Deflections of Reinforced Concrete Flexural Members. *Journal of the American Concrete Institute* , 637-674.

ACI Committee 445. (1998). Recent Approaches to Shear Design of Structural Concrete. *ASCE Journal of Structural Engineering , 124* (12).

Bentz, E. C. (2001, September). *Response-2000 Manual.* Retrieved April 18, 2010, from http://www.ecf.utoronto.ca/~bentz/manual2/final.pdf

Bentz, E. C. (2000). *Sectional Analysis of Reinforced Concrete Members.* University of Toronto, Department of Civil Engineering.

Biello, C., Bergman, L., & Kuchma, D. (2004). Experimental Investigation of a Small Scale Bridge Model Under a Moving Mass. *ASCE Journal of Structural Engineering , 130*, 799-804.

Caltrans. (2008). *Post-Tensioned Box Girder LRFD Design Example.* Prestressed Concrete Committee, Division of Engineering Services.

CEB-FIB. (1993). Model Code 1990. 437. Laussane: Comité Euro-International du Béton.

Chang, C. W., Lin, C. H., & Lien, S. L. (2009). Measurement radius of reinforcing steel bar in concrete using digital image GPR. *Construction and Building Materials* , 1057-1063.

Collins, M. P., & Mitchell, D. (1991). *Prestressed Concrete Structures.* Englewood Cliffs, New Jersey: Prentice Hall.

Gries, M., Giles, R., Kuchma, D., Spencer, B., & Bergman, L. (2010). *Advanced Bridge Capacity and Structural Integrity Assessment.* Final project report to USA-CERL (in progress), University of Illinois at Urbana-Champaign.

He, X.-Q., Zhu, Z.-Q., Liu, Q.-Y., & Lu, G.-Y. (2009). Review of GPR Rebar Detection. *PIERS Proceedings*, (pp. 804-813). Beijing.

Hegger, J. (2004). *ACI Structural Journal , 101* (2).

MacGregor, J. G., & Wight, J. K. (2005). *Reinforced Concrete: Mechanics and Design* (4th ed.). Upper Saddle River, NJ: Pearson Prentice Hall.

Minor, J., & Woodward, C. (1999). *Bridge Analysis Study, Phase II & Phase III.* New Mexico State University;.

Mitchell, D., & Collins, M. P. (1974). Diagonal Compression Field Theory - A Rational Model for Structural Concrete in Pure Torsion. *ACI Journal , 71* (8), 396-408.

NATO. (1990). Standard NATO Agreement 2021. *Computation of Bridge, Raft, Ferry, and Vehicle Classifications* .

Precast/Prestressed Concrete Institute. (2003). Chapter 7: Loads & Load Distribution. In *PCI Bridge Design Manual.* Chicago.

Ramirez, J. (2009). Recent Approaches to Shear Design. *ACI-ASCE Committee 445.*

Ray, J., & Butler, C. D. (2004, November). Rapid and Global Bridge Assessment for the Military. *ASCE JOURNAL OF BRIDGE ENGINEERING* .

Taly, N. (1998). *Design of Modern Highway Bridges.* New York: McGraw-Hill.

U.S. Army. (2002). FM3-34.343. *Military Nonstandard Fixed Bridging* . Washington DC: Headquarters, Department of the Army.

Van Groningen, C. N., & Paddock, R. A. (1997). *SmartBridge: A Tool for Estimating the Military Load Classification.* Argonne National Laboratory, Decision and Information Sciences Division, Argonne, IL.

Vecchio, F. (2000). Disturbed Stress Field Model for Reinforced Concrete: Formulation. *ASCE Journal of Structural Engineering , 126* (8), 1070-1077.

Vecchio, F. (2001). Disturbed Stress Field Model for Reinforced Concrete: Implementation. *ASCE Journal of Structural Engineering , 127* (1), 12-20.

Vecchio, F. J., & Collins, M. P. (1986, March-April). The Modified Compression-Field Theory for Reinforced Concrete Elements Subjected to Shear. *ACI Journal* , 219-231.

Vecchio, F., Lai, D., Shim, W., & Ng, J. (2001). Disturbed Stress Field Model for Reinforced Concrete: Validation. *ASCE Journal of Structural Engineering , 127* (4), 350-358.

Wickline, J. E., Cousins, T. E., & Seda-Sanabria, Y. (2003). *ERDC/GSL TR-03-12: A Study of Effective Moment of Inertia Models for Full-Scale Reinforced Concrete T-Beams Subjected to a Tandem-Axle Load Configuration.* Engineering Research and Development Center, Geotechnical and Structures Laboratory.

Wong, P., & Vecchio, F. J. (2002, August). *VecTor2 & Formworks User's Manual.* Retrieved April 18, 2010, from Vector Analysis Group: http://www.civ.utoronto.ca/vector/user_manuals/manual1.pdf

Zhan, R., & Xie, H. (2009). GPR measurement of the diameter of steel bars in concrete specimens based on the stationary wavelet transform. *Insight - Non-Destructive Testing and Condition Monitoring , 51* (3), 151-155.